JOURNAL OF GUIDANCE, CONTROL, AND DYNAMICS
Vol. 41, No. 5, May 2018

Biplane-Quadrotor Tail-Sitter UAV: Flight Dynamics and Control

Swati Swarnkar,* Hardik Parwana,† Mangal Kothari,‡ and Abhishek Abhishek§
Indian Institute of Technology Kanpur, Kanpur 208 016, Uttar Pradesh, India

DOI: 10.2514/1.G003201

This paper presents the development of 6-degrees-of-freedom (6-DOF) flight dynamics model and nonlinear control design for a novel hybrid biplane-quadrotor unmanned aerial vehicle capable of efficient operation in both vertical takeoff and landing (VTOL) mode and forward flight mode. The development of vehicle dynamics model considers a complete description of flight dynamics, wing aerodynamics, and prop wash modeling. Rotor and wing aerodynamics during hover, transition, and forward flight are the key components of the vehicle dynamics equations and are systematically validated with experimental data available in the literature. The rotor aerodynamic loads calculated using blade element theory and uniform inflow–based model is found to offer adequate fidelity during both axial and edgewise flights of the rotor. The rigid body rotation of 90° about pitch axis during transition from hover to forward flight and back necessitates the use of quaternions for representation of the attitude of the vehicle to avoid singularity associated with Euler angles for such maneuvers. A comprehensive nonlinear control design using dynamic inversion approach is developed for the whole flight regime that includes climb/descent, hover, transition, and forward flight. The performance of the proposed control design is demonstrated through numerical simulations on the 6-DOF model of the vehicle.

Nomenclature

A	=	rotor disk area, m^2
b	=	wing span, m
c	=	chord of rotor blade
C_{D_0}	=	profile drag of the UAV
C_{d_0}	=	zero lift drag coefficient of rotor blade airfoil
C_D, C_L	=	nondimensional drag and lift coefficients
C_{L_α}	=	lift curve slope, rad^{-1}
C_{l_α}	=	lift curve slope for rotor blade airfoil
C_T, C_Q	=	nondimensional thrust and torque coefficients
C_Y	=	nondimensional side force coefficient
$\bar{c}$	=	mean aerodynamic chord, m
D, L	=	drag and lift forces, N
d	=	moment arm of rotors, m
F	=	force, N
g	=	acceleration due to gravity, m/s^2
I	=	inertia, kg · m^2
$\bar{L}, M, N$	=	rolling, pitching, and yawing moments, N · m
m	=	mass of the vehicle, kg
N_b	=	number of blades in rotor
p, q, r	=	vehicle angular velocity components along quadrotor body axes, rad/s
R	=	rotor radius, m
S	=	wing area, m^2
T	=	thrust, N
u, v, w	=	vehicle velocity components along quadrotor body axes, m/s
V	=	vehicle velocity, m/s
V_{tip}	=	rotor tip speed, m/s
x, y, z	=	inertial position co-ordinates, m
Y	=	side force, N
α	=	wing angle of attack, rad
β	=	sideslip angle, rad
β_{0_i}	=	blade coning angle of ith rotor, rad
β_{1c_i}	=	cosine component of blade flap deflection of ith rotor, rad
β_{1s_i}	=	sine component of blade flap deflection of ith rotor, rad
η	=	quaternion attitude vector of quadrotor body frame with respect to inertial frame
λ_i	=	inflow factor of ith rotor
μ	=	advance ratio of the rotor
Ω	=	rotor angular speed, rad/s
θ_{0_i}	=	blade collective pitch angle of ith rotor, rad
θ_{tw}	=	linear twist rate for blade
θ_{75_i}	=	blade pitch angle at 75% of rotor radius, rad
ϕ, θ, ψ	=	Euler angles, rad
ρ	=	atmospheric air density, kg/m^3

Subscripts

a	=	due to aerodynamic forces
d	=	desired value
E	=	inertial frame
e	=	error value
Q	=	quadrotor body frame
t	=	due to thrust
W	=	wing body frame

I. Introduction

SMALL unmanned aerial vehicles (UAVs) are being used for mapping, surveillance, precision agriculture, payload delivery, and so on. Among these, the e-commerce sector is witnessing a dramatic shift toward the use of UAVs for delivering packages to remote areas faster and in an economically efficient way by traversing through air rather than land. Amazon, Google, Alibaba, and other e-commerce giants are already working on developing their own solutions for small payload delivery to cater to the "last mile." This can augment their profit by cutting labor cost. Beyond aerial logistics, these UAVs may also be useful for delivery of emergency supplies during disaster response, relief, and rehabilitation.

The development of UAVs has been traditionally focused on either fixed-wing or rotary-wing configurations. But the unique applications envisioned now require UAVs to fly efficiently like fixed wing and be able to take off, land, and hover like rotary wing vehicles to enable enhanced performance across the entire flight envelope. This requires out-of-the-box thinking and is inspiring development of novel hybrid

Presented as Paper 2018-1851 at the AIAA Science and Technology Forum and Exposition 2018, Kissimmee, FL, 8–12 January 2018; received 16 July 2017; revision received 30 November 2017; accepted for publication 3 December 2017; published online 29 January 2018.

*Graduate Student, Department of Aerospace Engineering.
†Undergraduate Student, Department of Aerospace Engineering.
‡Assistant Professor, Department of Aerospace Engineering; mangal@iitk.ac.in. Member AIAA.
§Assistant Professor, Department of Aerospace Engineering; abhish@iitk.ac.in. Member AIAA.

UAV concepts capable of vertical takeoff and landing (VTOL). Beyond the challenges associated with aerodynamic and structural design of these vehicles, the key to the success of these novel concepts lies in the development of a flight controller capable of stabilizing and controlling the vehicle during hover and forward flight regimes and also enable smooth transition between the two regimes. The operation of hybrid VTOL vehicles during hover and forward flight may require different sets of flight control strategies, making the control design very challenging.

The commonly studied hybrid VTOL concepts in the literature include monoplane wing tail-sitter [1–4], tiltrotor [5,6], compound helicopter, quad tiltrotor [7], and quad-tiltwing [8] concepts. The monoplane tail-sitter concept has the simplest design, but it suffers from poor control authority during hover due to use of a solitary propeller. The transition from hover to forward flight and back is quite challenging in such vehicles. The tail-sitter UAVs go through low-speed, high–angle-of-attack flight while performing agile maneuvers and also during transition from hover to forward flight. A detailed study of flight controller design for agile fixed-wing tail-sitter aircrafts is given in [9]. The work in [9] used flat plate aerodynamic theory to model aerodynamic forces and validated the model for hover and transition phase of the UAV by comparing the simulated results with experimental measurements. The transition to forward flight from hover condition is achieved primarily by manipulating the thrust and the control surface present in the wake of the propeller during hovering flight. It is therefore important to consider prop wash effect for executing effective transition maneuver as the prop wash induces significant airflow over the wing. The significance of including prop wash slipstream effect in UAV modeling is further emphasized in [10]. The acceleration and diffusion of slipstream are demonstrated through experiments, and an empirical relationship is established for the propeller slipstream in the absence of free stream velocity. In [3], the relevant model is studied and flight test results are presented for an autonomous fixed-wing aircraft with the capability to take off, hover, transition to and from level flight, and perch on a vertical landing platform. While the models described are used for control design, no validation of the model with flight test is presented. Systematic wind tunnel tests were carried out in [11,12] by measuring aerodynamic loads due to a propeller and wing at different angles of attack under oncoming flow to characterize aerodynamic performance of a tail-sitter vehicle to maintain equilibrium during transition. The idea of vertical bat tail-sitter UAV is presented as an alternative to conventional tail-sitter design in [4]. The concept uses thrust vectoring for control. Mimicking the V-22 Osprey tiltrotor design in small-sized UAVs is cumbersome as it requires use of swashplate for controlling the pitch angle of each of the rotors, making it mechanically complicated and therefore is only suitable for larger-sized UAVs as presented in [5]. The fixed-pitch propeller–based designs in [6] are easy to build but suffer from poor stability and control authority in pitch mode. Lift and thrust compounding results in high empty weight and therefore has not been attempted in low-weight class of UAVs.

The quad tiltrotor design has good control authority during hover and transition and its flight control is simpler than that for monoplane tail-sitter. But, the rotor wing interaction in hover and the aerodynamic interaction between fore and aft wings result in loss of efficiency. The interaction losses during hover for quad tiltrotor are addressed in the quad tiltwing design [8]. It has four rotors that are mounted on the four wings. The wings, together with the rotors, are tilted between vertical and horizontal configurations to accomplish vertical and horizontal flights. It hovers like a quadrotor and flies like a tandem wing airplane in forward flight mode. However, the transition from hover to forward flight and back offers significant challenges due to the flow separation on the wing operating at very large angle of attack at the beginning of the transition. The convertiplane design offers a better compromise with the part of wing under the downwash of rotor tilting with it to eliminate hover losses [13]. Also, the design facilitates easier transition, because significant portion of the wing remains straight at all times.

A more efficient hybrid UAV solution has been developed at University of Maryland, which is a quadrotor biplane tail-sitter micro air vehicle [12,14,15]. The design, in which two wings are attached in a biplane configuration to a conventional quadrotor consisting of counterrotating propellers, tries to overcome the lack of control authority of regular tail-sitter and mechanical complexity associated with tilting of rotors and wings in tiltrotor or tiltwing-type hybrid concepts by making use of the maneuverability of the vehicle for transition. This design is expected to offer significantly higher control authority and can successfully transition from hover to forward flight and back due to large moment arm between the four thrust vectors to enable aggressive maneuvering. This design offers better overall performance compared with some of the other options discussed above as it uses the same set of propellers for hover and forward flight. However, the use of battery power compromises its industrial usability. An enhanced design using an internal combustion engine and mechanical transmission of quadrotor biplane VTOL UAV is proposed in [16], which uses variable-pitch rotors instead of fixed-pitch ones to give high payload capacity, making it ideal solution for payload delivery applications. In this design, a variable-pitch H-shaped quadrotor design proposed in [17] is combined with two wings attached to the parallel limbs of the quadrotor in a biplane configuration similar to that of [14]. The key differences between the two designs are 1) the use of variable-pitch rotors instead of fixed-pitch ones, which enables use of internal combustion engine as its power plant; 2) significantly higher endurance in comparison to battery-powered solutions due to use of fuel engine; and 3) use of mechanical transmission to transfer power from engine to the rotors. The design is scalable but has complex transmission systems. In spite of this, the vehicle is preferred as it provides high endurance.

The control design for hover to forward flight transition for conventional single-propeller tail-sitter UAVs has been studied by several researchers [3,18–20]. Much of the early work on hybrid UAVs was concerned with developing individual controllers for different flight regimes and mostly linear controllers for transition between them [3,9,21]. However, the most challenging aspect of hybrid UAVs is the transition while considering the nonlinear dynamics. Many previous approaches involved a stall and stumble profile aimed at tossing the airplane between two different domains and working with linearized approximations. Recently, a combination of dynamic inversion and proportional integral derivative is developed for a tail-sitter UAV in [20]. This configuration uses canard surfaces and a shrouded propeller in pusher configuration for providing required moments. The control of tail-sitter UAVs with one or two propellers relies on controlling the thrust of the propeller and deflection of control surface in the prop wash. The attitude control is thus largely dependent on the slipstream of the propellers and the vehicle airspeed, and special care is needed to ensure sufficient control authority from the control surfaces such as elevator, ailerons, and canards [22]. Therefore, the control approaches developed for single-propeller tail-sitter UAVs cannot be employed for quadrotor tail-sitter [14,16]. The schematic of the vehicle is shown in Fig. 1.

Although significant work has been done on the design and aerodynamic analysis of the quadrotor biplane tail-sitter configuration, systematic development of flight dynamics model and control design has not been carried out. A detailed flight dynamics model of tail-sitter UAVs with longitudinal and lateral-directional coefficients is sparse in the literature. In this paper, a complete flight dynamics model is developed with description of geometric and aerodynamics parameters along with prop wash modeling. The model is validated using experimental data available in the literature. The paper also presents a comprehensive approach to design a set of nonlinear controllers for the complete mission profile of biplane-quadrotor UAV using nonlinear dynamic inversion. The UAV is seen as two different vehicles: quadrotor and fixed-wing airplane during vertical and horizontal phases of flight. The approach, although simplified, is still effective as the control design exercise can leverage the existing knowhow for two well-studied conventional air vehicles. The control design uses quaternion-based parameterization to avoid the singularity associated with Euler angle–based approach for 90° pitch rotation of tail-sitter aircrafts during hover-to-cruise transition. Two different body-fixed frames of reference are used during the entire flight regime for simple and effective control design.

The rest of the paper is structured as follows: A flight dynamics model of biplane-quadrotor is developed in Sec. II that cover kinematics, flight dynamics, aerodynamics, and rotor dynamics. A comprehensive

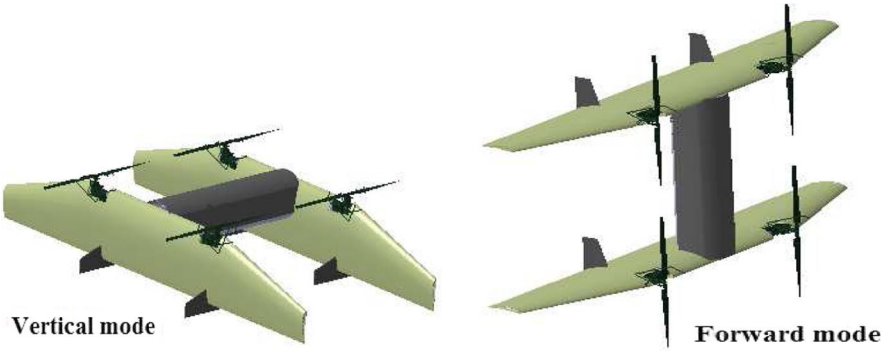

Fig. 1 Vertical and forward mode of the biplane-quadrotor UAV.

nonlinear control design using dynamic inversion approach is developed in Sec. III for the whole flight regime that includes climb/descent, hover, transition, and forward flight. The performance of the proposed control design is demonstrated through numerical simulation on 6-DOF model of the vehicle in Sec. IV and concluding remarks are given in Sec. V.

II. Flight Dynamics Model

In this section, a physics-based flight dynamics model of biplane-quadrotor UAV is developed. Before getting into the details of the model, it is important to appreciate the fact that in the absence of any fixed-wing control surfaces, the control of quadrotor tail-sitter UAV is completely governed by regulating thrust of the four variable-pitch rotors. The modeling of rotor thrust and torque during hover flight and axial climb-like flight (airplane-like cruise mode) can be accomplished by means of blade element theory (BET) along with momentum theory for inflow calculation. As the UAV transitions to forward flight from hover, the state of rotor changes from hover condition to edgewise flight as vehicle pitch attitude changes through 90°. After the completion of transition, the rotor returns back to axial climb condition when the UAV is under steady-level forward flight. The accurate estimation of rotor and wing aerodynamic forces during the transition and under the influence of prop wash is the key challenge toward accurate flight dynamic modeling of this UAV. In the current study, the rotor forces and moments during edgewise flight are calculated, with the assumption of flap-only dynamics for rotor blades, using BET and momentum theory for inflow. It should be noted that the inflow calculation using momentum theory for hover and axial climbing flight results in closed form analytical expressions. But, for the edgewise flight, the inflow equation becomes nonlinear and therefore has to be solved iteratively using Newton–Raphson or fixed-point iteration as discussed later. First, the strategy required for primary control of this UAV is discussed followed by detailed development of the mathematical model that includes flight dynamics, wing aerodynamics, and rotor dynamics.

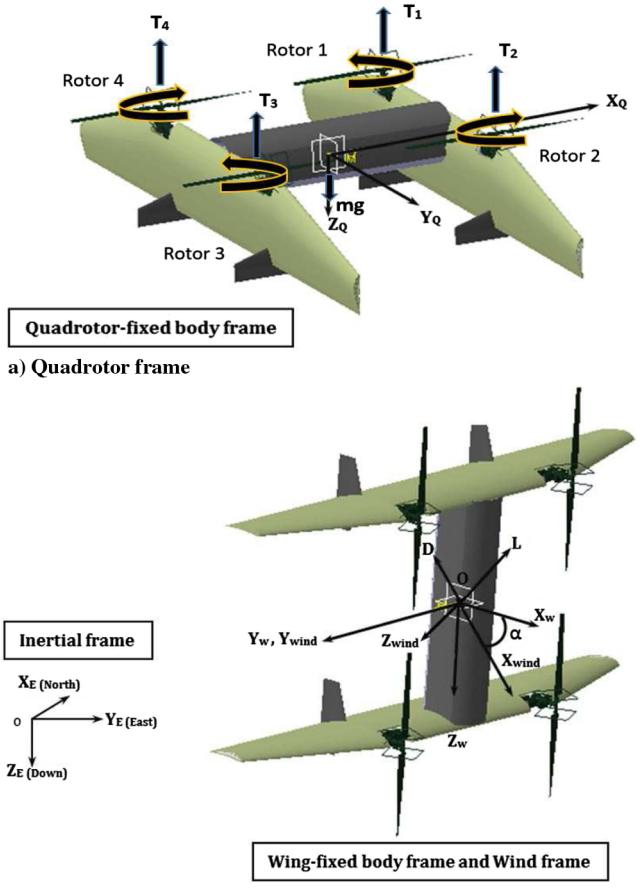

Fig. 2 Biplane reference frames.

A. Strategy of Control

The current tail-sitter UAV operates in three flight regimes: 1) VTOL or quadrotor; 2) transition; and 3) fixed-wing or forward flight. In the quadrotor mode, the up/down motion is easily controlled by collectively increasing or decreasing the collective pitch angles for all the rotors/propellers simultaneously. Forward and side-ward flight can be achieved by controlling pitching and rolling moments. Positive roll of a quadrotor in H-configuration (Fig. 2a) can be achieved by providing higher thrust to rotors 1 and 4, and correspondingly lower thrust to rotors 2 and 3. Similarly, positive pitch can be achieved by providing higher thrust to rotors 1 and 2, and correspondingly lower thrust to rotors 3 and 4. The yaw control is less intuitive. A nonzero net torque along the Z_Q axis causes yawing motion that can be generated from the drag force acting on each rotor. The collective pitch of the two diagonal rotors rotating in the same direction is increased and the collective pitch of the other diagonal pair is reduced to generate pure yaw motion.

The control of transition is crucial and challenging as the vehicle does not have enough forward speed to generate adequate lift for supporting the entire weight of the UAV. A conceptual idea of transition is demonstrated in Fig. 3. The vehicle is initially commanded to change its pitch orientation by 90° from the vertical orientation of rotors and wings to the orientation for the horizontal flight where both rotors and wings are nearly horizontal. Because no conventional control surfaces are present, the control moments need to be generated by the four rotors. When aerodynamic forces contributed by the wing become significant, the fixed-wing aerodynamics becomes prominent, but the UAV translational and rotational motions are still controlled using the forces and moments generated by the rotors for this tailless configuration having no control surfaces.

The third part, forward flight, is similar to conventional fixed-wing mode. The mechanism to generate pitching moment during this mode remains the same as the quadrotor mode. It should be noted that,

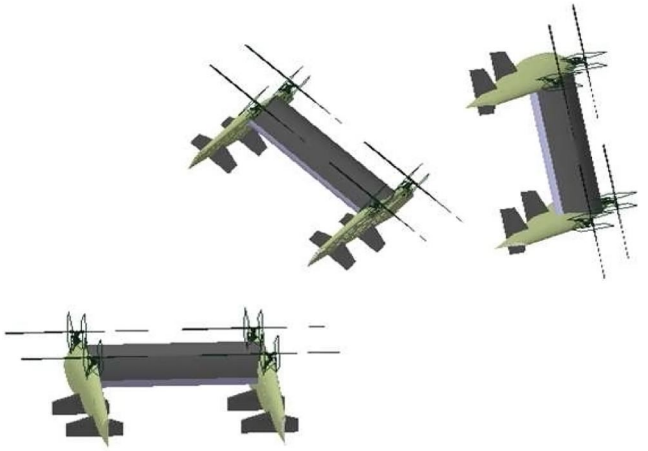

Fig. 3 Transition from hover (vertical) to forward flight (horizontal) mode.

after the vehicle maneuvers into the forward flight mode, the yaw and roll degree of freedom during hovering flight becomes the roll and yaw degree of freedom, respectively, as shown in Fig. 2b. The flight control for various motions can be achieved as explained earlier. In addition, the pitching moment contribution from the wings can be compensated by differential thrust generation by the top and bottom rotors, during forward flight. It is important to emphasize that the rotors operate at reduced RPM in forward flight compared with VTOL mode to ensure high efficiency during forward flight.

B. Vehicle Equation of Motion

A mathematical model of biplane-quadrotor tail-sitter UAV in the body axis can be derived by fixing the right-hand coordinate axis either with respect to conventional wing frame (see Fig 2b) or with respect to conventional quadrotor frame as shown in Fig. 2a. Because most of the flight phases, that is, vertical takeoff, hover, initial transition, and landing, are performed in VTOL mode, the wing aerodynamic forces under this condition are generated primarily due to prop wash because of low translational speeds. Therefore, it is more convenient to describe dynamics of this UAV in the quadrotor frame. In addition, the derivation of control law for all these flight phases becomes relatively simple if reference body frame is chosen to be the quadrotor frame. The equations of motion are standard 6-degrees-of-freedom (6-DOF) equations [23,24]; however, the major difference is in control moment generation, which is achieved by rotors alone instead of control surfaces, which needs to be included for this unconventional configuration.

1. Flight Dynamics

The forces acting on the UAV consist of gravitational, aerodynamic (lift and drag), and propulsive forces, which can be resolved along the quadrotor body axis. Similarly, the total moment acting is due to contribution from aerodynamic and propulsive forces. The translational and rotational dynamic equations are given as

$$\begin{bmatrix}\dot{u}\\ \dot{v}\\ \dot{w}\end{bmatrix} = \begin{bmatrix}0\\ 0\\ -T/m\end{bmatrix} + \begin{bmatrix}F_{ax}/m\\ F_{ay}/m\\ F_{az}/m\end{bmatrix} + g\begin{bmatrix}2\eta_1\eta_3 - 2\eta_0\eta_2\\ 2\eta_2\eta_3 + 2\eta_0\eta_1\\ \eta_0^2 - \eta_1^2 - \eta_2^2 + \eta_3^2\end{bmatrix} + \begin{bmatrix}rv - qw\\ pw - ru\\ qu - pv\end{bmatrix} \tag{1}$$

$$\begin{bmatrix}\dot{p}\\ \dot{q}\\ \dot{r}\end{bmatrix} = \begin{bmatrix}(c_1 r + c_2 p)q + c_3(\bar{L}_a + \bar{L}_t) + c_4(N_a + N_t)\\ c_5 pr - c_6(p^2 - r^2) + c_7(M_a + M_t)\\ (c_8 p - c_2 r)q + c_4(\bar{L}_a + \bar{L}_t) + c_9(N_a + N_t)\end{bmatrix} \tag{2}$$

where all the variables are referred with respect to quadrotor frame and $\eta \triangleq [\eta_0 \quad \eta_1 \quad \eta_2 \quad \eta_3]^T$, η_0 and $[\eta_1 \quad \eta_2 \quad \eta_3]$ represent the scalar and vector parts, respectively. The aerodynamic forces in the quadrotor frame can be obtained from wind axes forces as

$$\begin{bmatrix}F_{ax}\\ F_{ay}\\ F_{az}\end{bmatrix} = \begin{bmatrix}\sin\alpha\cos\beta & -\sin\alpha\sin\beta & \cos\alpha\\ \sin\beta & \cos\beta & 0\\ -\cos\alpha\cos\beta & \cos\alpha\sin\beta & \sin\alpha\end{bmatrix}\begin{bmatrix}-D\\ Y\\ -L\end{bmatrix}$$

The moments due to aerodynamic forces and thrust are defined later in this section. The constants c_i represent inertia terms:

$$\begin{bmatrix}c_1\\ c_2\\ c_3\\ c_4\\ c_8\\ c_9\end{bmatrix} = \frac{1}{I_x I_z - I_{xz}^2}\begin{bmatrix}(I_y - I_z)I_z - I_{xz}^2\\ (I_x - I_y + I_z)I_{xz}\\ I_z\\ I_{xz}\\ (I_x - I_y)I_x + I_{xz}^2\\ I_x\end{bmatrix}$$

$$\begin{bmatrix}c_5\\ c_6\\ c_7\end{bmatrix} = \frac{1}{I_y}\begin{bmatrix}(I_z - I_x)\\ I_{xz}\\ 1\end{bmatrix}$$

The true airspeed and dynamic pressure are defined as

$$V = \sqrt{u^2 + v^2 + w^2}$$
$$Q_\infty = 0.5\rho V^2$$

2. Kinematics

The kinematic equations relate the displacement and rate vectors defined in different coordinate frames (inertial and quadrotor body frames). The relation between derivative of quaternions [25,26] defined with respect to inertial frame and the angular velocity vector of body frame with respect to inertial frame is given by

$$\begin{bmatrix}\dot{\eta}_0\\ \dot{\eta}_1\\ \dot{\eta}_2\\ \dot{\eta}_3\end{bmatrix} = \frac{1}{2}\begin{bmatrix}-\eta_1 & -\eta_2 & -\eta_3\\ \eta_0 & -\eta_3 & \eta_2\\ \eta_3 & \eta_0 & -\eta_1\\ -\eta_2 & \eta_1 & \eta_0\end{bmatrix}\begin{bmatrix}p\\ q\\ r\end{bmatrix} \tag{3}$$

The vehicle velocity vector in quadrotor body frame is related to the same vector in inertial frame by transformation matrix

$$\begin{bmatrix}\dot{x}\\ \dot{y}\\ \dot{z}\end{bmatrix} = R_B^E(\eta)\begin{bmatrix}u\\ v\\ w\end{bmatrix} \tag{4}$$

where

$$R_B^E(\eta) = \begin{bmatrix}\eta_0^2 + \eta_1^2 - \eta_2^2 - \eta_3^2 & 2\eta_1\eta_2 - 2\eta_3\eta_0 & 2\eta_1\eta_3 + 2\eta_2\eta_0\\ 2\eta_1\eta_2 + 2\eta_3\eta_0 & \eta_0^2 - \eta_1^2 + \eta_2^2 - \eta_3^2 & 2\eta_2\eta_3 - 2\eta_0\eta_1\\ 2\eta_1\eta_3 - 2\eta_2\eta_0 & 2\eta_2\eta_3 + 2\eta_1\eta_0 & \eta_0^2 - \eta_1^2 - \eta_2^2 + \eta_3^2\end{bmatrix} \tag{5}$$

3. Geometric and Aerodynamics Parameters

The main objective of our research is to develop a nonlinear control strategy for biplane-quadrotor tail-sitter UAV concept proposed in [16]. The geometric and inertia parameters of this UAV are summarized in Table 1. The work in [16] focused on rotor and wing design and structural analysis to meet the desired performance objectives during hover and forward flight; it did not explore the flight dynamic modeling. The calculation of aerodynamic

Table 1 Geometric and inertia parameters

Parameters	Mass	Wing span	Wing area (single)	Root chord	Tip chord	Aspect ratio
Values	12 kg	2.29 m	0.754 m^2	0.39 m	0.176 m	6.9
Parameters	Gap-to-chord ratio	X_{cg}	X_{ac}	I_x	I_y	I_z
Values	2.56	0.157 m	0.0838 m	1.86 kg · m^2	2.031 kg · m^2	3.617 kg · m^2

Table 2 Nondimensional longitudinal and lateral/directional aerodynamic derivatives

Parameters	C_{D_0}	C_{L_0}	C_{L_α}	C_{L_q}	C_{m_0}	C_{m_α}	C_{m_q}	C_{Y_β}
Values	0.009	0.4918	4.695	0	−0.0156	0.995	−0.51	−0.951
Parameters	C_{Y_p}	C_{Y_r}	C_{l_β}	C_{l_p}	C_{l_r}	C_{n_β}	C_{n_p}	C_{n_r}
Values	0	0.008	0	−0.43	0.29	0.0812	−0.4044	−0.05

derivatives for the forward flight mode of the UAV is done as a preliminary study to determine the contribution of various quantities to overall vehicle forces and moments. The well-established equations based on Datcom [27,28] are used for this purpose. Because the present model is an unconventional configuration, certain assumptions have to be made, and only the terms expected to make the most significant contribution have been considered. For example, the interference between the wings is neglected due to presence of significant spacing. However, as discussed in the validation section later, the values provided in Table 2 provide realistic physical representation of the system being studied. The modeling of prop wash effect is discussed later in this section. More accurate estimates of the derivatives can be obtained by using flight test data or wind tunnel testing.

C. Wing Aerodynamics

The gap-to-chord ratio (g/c) of the vehicle is significantly high, and hence the interference between the wings is neglected for analytical purposes. The aerodynamic force and moment coefficients of the biplane-quadrotor UAV can be calculated first for a single wing and then the effect of the other wing can be added to get the combined effect. The nondimensional nonlinear lift coefficient [23] is given by

$$C_L = C_L(\alpha) + C_{Lq}\frac{q_W \bar{c}}{2V} \tag{6}$$

where $C_L(\alpha) = (1 - \sigma(\alpha))[C_{L0} + C_{L\alpha}\alpha] + \sigma(\alpha)[2\text{sign}(\alpha)\sin^2(\alpha)\cos(\alpha)]$ and

$$\sigma(\alpha) = \frac{1 + e^{-M_0(\alpha-\alpha_0)} + e^{M_0(\alpha+\alpha_0)}}{(1 + e^{-M_0(\alpha-\alpha_0)})(1 + e^{M_0(\alpha+\alpha_0)})}$$

The above sigmoid function blends a linear lift coefficient with flat plate lift model with cutoff at $\pm\alpha_0$ with transition rate M_0. The nondimensional drag coefficient is given by

$$C_D = C_{D_0} + kC_L^2 \tag{7}$$

where C_{D_0} is the overall profile drag of UAV. The total side force coefficient is given by

$$C_Y = C_{Y_\beta}\beta + C_{Y_p}\frac{p_W b}{2V} + C_{Y_r}\frac{r_W b}{2V} \tag{8}$$

The total rolling, pitching, and yawing moment coefficients due to aerodynamic forces about wing fixed axes in nondimensional form are modeled as

$$\left.\begin{aligned} C_l &= C_{l_\beta}\beta + C_{l_p}\frac{p_W b}{2V} + C_{l_r}\frac{r_W b}{2V} \\ C_m &= C_{m_0} + C_{m_\alpha}\alpha + C_{m_q}\frac{q_W \bar{c}}{2V} \\ C_n &= C_{n_\beta}\beta + C_{n_p}\frac{p_W b}{2V} + C_{n_r}\frac{r_W b}{2V} \end{aligned}\right\} \tag{9}$$

D. Rotor Aerodynamics

In variable-pitch quadrotors, thrust from each rotor is varied by changing its collective pitch input [29]. The four rotors are mounted in the form of an "H"-shaped quadrotor configuration, where each pair of arms of the quadrotor is placed along the wings and the central part of the quadrotor forms the fuselage of the UAV. The aerodynamic loads generated by the rotor (thrust, drag, and torque) can be calculated using the BET along with the momentum theory [30] as described below. The contribution of each blade element to the total aerodynamic load (lift, drag, and pitching moment) is calculated and then integrated over the blade radius to calculate the net rotor thrust, rotor drag, and torque contribution of each blade, which is then multiplied with the number of blades to calculate the total thrust and torque from each rotor. For the hover condition, the nondimensional thrust coefficient, C_{T_i}, and torque coefficient, C_{Q_i}, for the ith rotor using the approach given in [30] are

$$C_{T_i} = \frac{1}{2}\sigma C_{l_\alpha}\left(\frac{\theta_{0_i}}{3} - \frac{\lambda_i}{2}\right) \tag{10}$$

$$C_{Q_i} = \frac{1}{2}\sigma\left(\frac{\lambda_i C_{l\alpha}\theta_{0_i}}{3} - \frac{\lambda_i^2 C_{l_\alpha}}{2} + \frac{C_{d_o}}{4}\right) \tag{11}$$

where $\sigma = N_b c/\pi R$ is rotor solidity. For a blade with linear twist (θ_{tw}), θ_{0_i} may be replaced with θ_{75_i}, which is the blade pitch angle at 75% of rotor radius. It should be noted that there is no in-plane rotor drag force during hover condition. These nondimensional quantities can be converted to corresponding dimensional parameters by using $T_i = C_{T_i}\rho A V_{\text{tip}}^2$ and $Q_i = C_{Q_i}\rho A R V_{\text{tip}}^2$, where $V_{\text{tip}} = \Omega R$ is the tip speed of rotor blade. The only unknown parameter in Eqs. (10) and (11) is the inflow ratio λ_i, which can be evaluated using momentum theory for the hovering flight condition using the following relationship:

$$\lambda_i = \sqrt{\frac{C_{T_i}}{2}} \tag{12}$$

Substituting the value of λ_i in Eq. (10) gives

$$C_{T_i} = \frac{1}{2}\sigma C_{l\alpha}\left(\frac{\theta_{0_i}}{3} - \frac{1}{2}\sqrt{\frac{C_{T_i}}{2}}\right) \tag{13}$$

After rearranging, we get

$$\theta_{0_i} = \frac{6C_{T_i}}{\sigma C_{l\alpha}} + \frac{3}{2}\sqrt{\frac{C_{T_i}}{2}} \tag{14}$$

Substituting the above pitch angle and inflow ratio in Eq. (11) gives

$$C_{Q_i} = \frac{1}{2}\sigma\left(\frac{\sqrt{2}C_{T_i}^{3/2}}{\sigma} + \frac{C_{d_{o_i}}}{4}\right) \tag{15}$$

From the above definitions of thrust and torque, it can be seen that

$$T_i = KC_{T_i} \tag{16}$$

$$Q_i = KRC_{Q_i} \tag{17}$$

where $K = \rho A V_{\text{tip}}^2$ is typically constant for the variable-pitch quadrotor as the rotor speed is regulated about a prescribed constant value.

As the UAV transitions to forward flight from hover, the state of rotor changes from hover condition to edgewise flight as vehicle pitch attitude changes by 90°. After the completion of transition, the rotor returns back to axial climb condition when the UAV is under steady-level forward flight. The rotor loads need to be calculated using the following approach based on BET and uniform inflow. If α_s represents the angle made by rotor shaft with the vertical direction at any time during the transition from hover to forward flight, then using the momentum theory, the total inflow through the ith rotor in rotor tip path plane (λ_{TPP_i}) is given by

$$\lambda_{\text{TPP}_i} = \mu\tan\alpha_s + \frac{C_{T_i}}{\sqrt{\mu^2 + \lambda_{\text{TPP}}^2}} \tag{18}$$

where $\mu = V\cos\alpha_s/\Omega R$. The inflow in the hub plane during edgewise flight is given by $\lambda_{h_i} = \lambda_{\text{TPP}_i} - \mu\beta_{1c_i}$, where β_{1c_i} for the ith rotor, it is given by

$$\beta_{1c_i} = -\frac{(8/3)\mu(\theta_{0_i} - 0.75\lambda_{\text{TPP}} + 0.75\theta_{\text{tw}})}{1 - 0.5\mu^2} \tag{19}$$

The above equation of cosine component of flap deflection is obtained by solving the blade flap equation [30] for a rotor without cyclic inputs. Likewise, the sine component (β_{1s_i}) is given by

$$\beta_{1s_i} = -\frac{4\mu\beta_0}{3(1 + 0.5\mu^2)} \tag{20}$$

The thrust, drag force, and torque produced by the rotor during the edgewise flight are given by the following equations, respectively,

$$C_{T_i} = 0.5\sigma C_{l_\alpha}\left[\frac{1}{3}\theta_{0_i}(1 + 1.5\mu^2) + 0.25\theta_{\text{tw}}(1 + \mu^2) - 0.5\lambda_{h_i}\right] \tag{21}$$

$$C_{H_i} = 0.5\sigma C_{l_\alpha}\left[0.5\mu\lambda_{h_i}(\theta_{0_i} + 0.5\theta_{\text{tw}}) + 0.25\mu\beta_{0_i}^2 - \beta_{1c_i}\left(\frac{\theta_0}{3} + \frac{\theta_{\text{tw}}}{4}\right)\right] + 0.25\sigma C_{d_0}\mu \tag{22}$$

$$C_{Q_i} = 0.5\sigma C_{l_\alpha}\left[\frac{\lambda_{h_i}\theta_0}{3} + 0.25\lambda\theta_{\text{tw}} - 0.5\lambda^2 - 0.125(\beta_{1c}^2 + \beta_{1s}^2)\right] + 0.125C_{d_o}(1 + \mu^2) \tag{23}$$

where β_0 for $i^t h$ rotor is given by

$$\beta_{0_i} = \gamma\left[\frac{1}{8}(\theta_{0_i}(1 + \mu^2) - \frac{1}{6}\lambda_{\text{TPP}} + 0.1\theta_{\text{tw}}\left(1 + \frac{5}{6}\mu^2\right)\right] \tag{24}$$

Equation (18) is a nonlinear equation and can be solved iteratively using Newton–Raphson method; the solution converges quickly in three to four steps. Therefore, Eqs. (18–24) have to be solved iteratively to obtain the rotor inflow, thrust, torque, and drag force. The inflow thus calculated (λ_h) is used to obtain prop wash velocity ($v = \lambda\Omega R$) in the next subsection to account for the prop wash effect on net wing lift, during the transition flight.

E. Prop Wash Model

The transition flight of a tail-sitter UAV from hover to forward flight is a high angle-of-attack maneuver. The wings used in the UAV have relatively short aspect ratio and the rotor radius is significantly large; therefore, the rotor down wash is expected to have significant effect on the wing aerodynamic loads during transition and forward flight. However, unlike typical tail-sitter aircrafts, the biplane-quadrotor vehicle does not have any conventional aircraft control surfaces; therefore, the effect of rotor/prop wash on control surfaces is not considered. The air velocity in the prop wash during transition and forward flight can be computed easily using the momentum theory. The calculation based on the momentum theory is adequate because the total rotor wash is dominated by the high value of uniform total inflow due to forward speed of the UAV during forward flight, which is significantly higher than the nonuniform velocity induced by the rotor. The calculation of prop wash can be calculated using the momentum theory as described below. From the momentum theory, the hover-induced velocity ($v_h = \lambda\Omega R$) is given by [same as Eq. (12)]

$$v_h = \sqrt{\frac{T}{2\rho A}} \tag{25}$$

Here, the value of T can be computed from either the control algorithm or BET. Depending on the mode of flight, the value of thrust can be chosen to be equal to the thrust required for hover or constant-speed vertical climb or constant-speed forward flight. In case of constant-speed forward flight, this thrust corresponds to the value required to overcome the drag of the UAV. Depending on whether it is climbing flight during hover mode or forward flight, the induced velocity for axial climbing flight is given by

$$v = v_h\left(-\frac{V}{2v_h} + \sqrt{\left(\frac{V}{2v_h}\right)^2 + 1}\right) \tag{26}$$

Next, for computing the net aerodynamic loads acting on the wing, the entire wing can be divided into two zones: 1) wing area in the rotor/prop wash, and 2) wing area out of prop wash. The net lift on the wing can be calculated by adding the lift contributions from both segments. The velocity and angle of attack in the prop wash affected segment are calculated by performing the vector sum of the free stream velocity (V) with the prop wash velocity (v) [9]. The net wing lift with the inclusion of prop wash effect is thus given by

$$L = \frac{1}{2}\rho V^2 S_{nw} C_{L_{nw}} + \frac{1}{2}\rho V_p^2 S_w C_{L_w} \tag{27}$$

where $V_p = \sqrt{V^2 + v^2 + 2Vv\cos\alpha}$, $\alpha_p = \tan^{-1}(V\sin\alpha/v + V\cos\alpha)$. $C_{L_{nw}}$ and C_{L_w} are computed using Eq. (6). Here, "nw" represents without prop wash and "w" represents with prop wash. Similarly,

the net drag and pitching moment under influence of prop wash can be estimated. The total drag force is given by

$$D = \frac{1}{2}\rho V^2 S_{\text{nw}} C_{D_{\text{nw}}} + \frac{1}{2}\rho V_p^2 S_w C_{D_w} \tag{28}$$

where $C_{D_{\text{nw}}} = C_{D_{0_{\text{nw}}}} + kC_{L_{\text{nw}}}^2$ and $C_{D_w} = C_{D_{0_w}} + kC_{L_w}^2$. The moments due to aerodynamic forces about wing axes are defined as

$$\begin{bmatrix} \bar{L}_a \\ M_a \\ N_a \end{bmatrix}_W = \begin{bmatrix} 0.5\rho V^2 SbC_l \\ 0.5\rho\bar{c}[V^2 S_{\text{nw}}(C_{m_0} + C_{m_{\alpha_{\text{nw}}}}\alpha) + V_p^2 S_w(C_{m_0} + C_{m_{\alpha_w}}\alpha_p)] \\ 0.5\rho V^2 SbC_n \end{bmatrix}_W \tag{29}$$

F. Validation of Rotor and Wing Aerodynamics

The rotor and wing aerodynamics models discussed in the previous sections are validated using the experimental data available in the literature [12,17] before carrying out the control design. The most critical element of the flight dynamic modeling of a rotary wing UAV is the aerodynamic model of the rotor itself. Therefore, the BET formulation used for rotor thrust and torque calculation in hover is validated using the experimental data available for small variable-pitch rotor [17]. Figures 4a and 4b compare the measured and predicted thrust and torque, respectively, for a rotor of 0.355 m radius and 0.32 m chord and symmetric rotor blades for two different RPMs. The predictions using the current BET formulation with uniform inflow show excellent correlation with the experimental data.

There is dearth of flight test data for complete tail-sitter UAVs. However, [12] conducted systematic wind tunnel tests on isolated fixed-pitch propeller/rotor and propeller–wing combination to estimate the loads encountered by the propeller and propeller–wing system during transition flight by varying the orientation of the wing from near-horizontal to near-vertical position. During this experiment, the net horizontal force and vertical force generated by only the propeller and then propeller and wing together in the presence of free stream velocity of 6.2 m/s was measured using a six-component load cell. The experiment setup described in [12] is simulated using the analysis presented in this section. The comparison of variation of horizontal and vertical forces due to propeller alone, which is a combination of rotor thrust and rotor drag forces, is shown in Fig. 5a. The current BET-based analysis for edgewise flight of the rotor shows excellent agreement with the experimental data. The incorporation of the wing lift model (with the prop wash effect included) used in the current paper also shows satisfactory correlation with the trends observed for the horizontal and vertical forces in the presence of wing. However, at high shaft angles representative of wing in near-vertical position, the current analysis overpredicts the vertical force. This may possibly be because, in the experiments performed in [12], the propeller is mounted slightly above the wing top surface and it is not symmetrically placed; therefore, at very high wing angle of attack the free stream is blocked by the wing and the propeller wash is mostly directed over the wing top surface, resulting in decrease in suction and hence reduction in measured lift. This is further justified

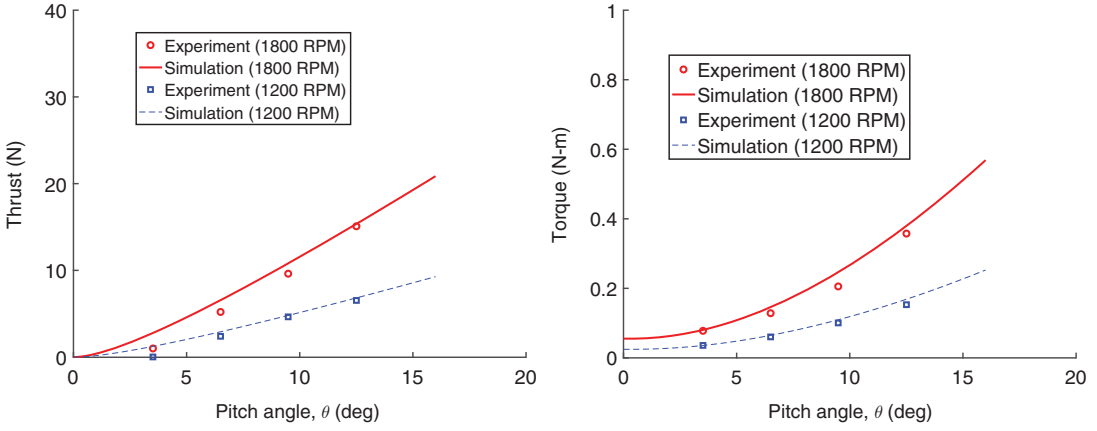

a) Thrust vs. Pitch angle b) Torque vs. Pitch angle

Fig. 4 Validation of thrust and torque prediction from the blade element theory analysis in hover; experimental data are from [17].

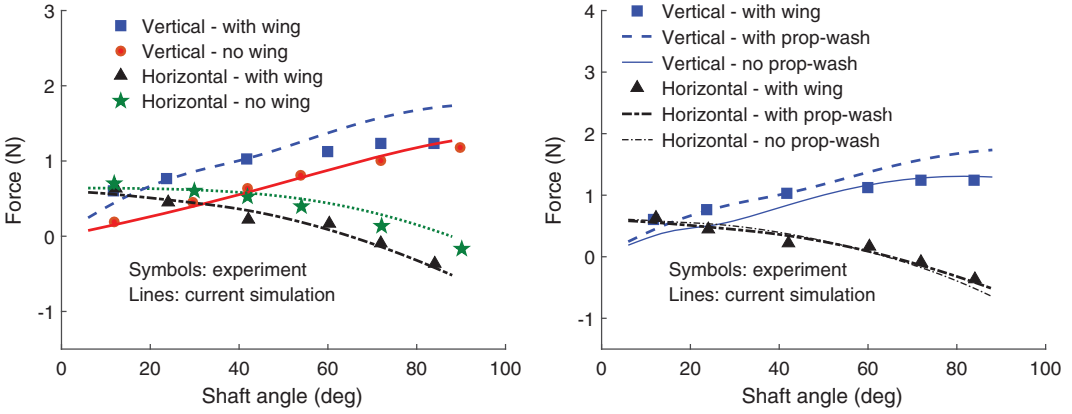

a) Propeller and wing loads b) Effect of prop wash

Fig. 5 Validation of rotor and wing loads calculation during transition flight; experimental data are from [12].

by the fact that at such high angles of attack (>45°) the vertical force predicted without the prop wash effect shows better correlation than that with the prop wash effect (see Fig. 5b). Figure 5b further highlights the importance of modeling prop wash, which has significant influence on vertical force (lift) and less significant influence on drag. In this paper, prop wash is incorporated for the calculation of the aerodynamic loads generated by the wing.

III. Control Design

In this section, we develop control laws for vertical/hover, transition, and fixed-wing modes of biplane-quadrotor UAV using nonlinear dynamic inversion [31]. Similar to the majority of aerospace vehicles, the biplane-quadrotor is underactuated. This means that the vehicle needs to control its position and attitude through four control inputs. For VTOL and fixed-wing modes, the control laws are designed in two loops: outer and inner loops. The outer loop works on translational dynamics and generates the desired thrust, pitch, and yaw/roll angles. The inner loop works on rotational dynamics and generates the desired pitch, roll, and yaw moments to meet the requirement of the outer loop. The transition mode is controlled by inner loop with altitude hold as the interest is to control pitch attitude rather than position. To meet the requirement of thrust and moments, a third loop is introduced that dynamically allocates control to each rotor. This is because there is a nonlinear relation between moment and thrust coefficients.

A. Quadrotor Mode

During vertical takeoff, hover, initial transition, and landing phases, no significant aerodynamic forces and moments are generated by the wings. Hence, the vehicle is considered to be in quadrotor mode. It is advantageous to derive the control law by assuming that the total forces and moments that act on the vehicle are only due to thrust. The controller during this mode is derived using the dynamic model defined in the quadrotor frame. However, we consider the effect of prop wash in the flight dynamic model.

1. Outer Loop Design

In the quadrotor mode, which essentially consists of a vertical/hover flight phase, the significant forces acting on the body are thrust and gravity. The aerodynamic forces can be assumed to be insignificant because of very low velocity required during these phases of flight. The translational dynamics in the inertial frame of reference is given by Newton's second law as

$$m\begin{bmatrix}\ddot{x}\\ \ddot{y}\\ \ddot{z}\end{bmatrix}=\begin{bmatrix}0\\ 0\\ mg\end{bmatrix}+\begin{bmatrix}\cos\theta\cos\psi & \sin\phi\sin\theta\cos\psi-\cos\phi\sin\psi & \cos\phi\sin\theta\cos\psi+\sin\phi\sin\psi\\ \cos\theta\sin\psi & \sin\phi\sin\theta\sin\psi+\cos\phi\cos\psi & \cos\phi\sin\theta\sin\psi-\sin\phi\cos\psi\\ -\sin\theta & \sin\phi\cos\theta & \cos\phi\cos\theta\end{bmatrix}\begin{bmatrix}0\\ 0\\ -T\end{bmatrix} \tag{30}$$

The above second-order translational dynamics is relatively slower as compared with the rotational dynamics. Hence, it is used for the outer loop flight control system design. The desired translational error dynamics is chosen as

$$(\ddot{X}-\ddot{X}_d)+2\zeta_X\omega_{n_X}^T(\dot{X}-\dot{X}_d)+\omega_{n_X}\omega_{n_X}^T(X-X_d)=0 \tag{31}$$

where $X\triangleq[x\quad y\quad z]^T$. ζ_X and ω_{n_X} represent 3×3 diagonal matrices of the desired damping ratio and natural frequency, respectively. The desired thrust, pitch, and roll angles can be computed by combining Eqs. (30) and (31) as follows [32]:

$$T_d=m\sqrt{\ddot{x}^2+\ddot{y}^2+(g-\ddot{z})^2} \tag{32}$$

$$\phi_d=\sin^{-1}\left[\frac{-m\ddot{x}\sin\psi_d+m\ddot{y}\cos\psi_d}{T_d}\right] \tag{33}$$

$$\theta_d=\sin^{-1}\left[\frac{-m\ddot{x}\cos\psi_d-m\ddot{y}\sin\psi_d}{T_d\cos\phi_d}\right] \tag{34}$$

The desired quaternion vector can now be determined as

$$\eta_d=\begin{bmatrix}\cos(\phi_d/2)\cos(\theta_d/2)\cos(\psi_d/2)+\sin(\phi_d/2)\sin(\theta_d/2)\sin(\psi_d/2)\\ \sin(\phi_d/2)\sin(\theta_d/2)\cos(\psi_d/2)-\cos(\phi_d/2)\sin(\theta_d/2)\sin(\psi_d/2)\\ \cos(\phi_d/2)\sin(\theta_d/2)\cos(\psi_d/2)+\sin(\phi_d/2)\cos(\theta_d/2)\sin(\psi_d/2)\\ \cos(\phi_d/2)\cos(\theta_d/2)\sin(\psi_d/2)-\sin(\phi_d/2)\sin(\theta_d/2)\cos(\psi_d/2)\end{bmatrix} \tag{35}$$

2. Inner Loop Design

In this subsection, we propose a control law for attitude tracking based on the quaternion error dynamics. The rotational dynamics of the vehicle is faster as compared with the translational dynamics. The rotational dynamics and kinematics equations in the quadrotor body-fixed frame can be written as

$$\tau_t=I\dot{\boldsymbol{\omega}}+\boldsymbol{\omega}\times I\boldsymbol{\omega} \tag{36}$$

$$\boldsymbol{\omega}=2G(\eta)\dot{\eta} \tag{37}$$

where the total moments acting on the UAV during quadrotor mode are assumed to be due to only thrust forces for control design. However, the effects of wing aerodynamics, including prop wash, are taken into account while propagating the vehicle states. The variable τ_t represents the moment vector about the quadrotor body axes, $\boldsymbol{\omega}$ represents the angular velocity vector of the quadrotor frame with respect to the inertial frame expressed in the quadrotor frame, I is the inertia matrix, and $G(\eta)$ is given by

$$G(\eta)=\begin{bmatrix}-\eta_1 & \eta_0 & \eta_3 & -\eta_2\\ -\eta_2 & -\eta_3 & \eta_0 & \eta_1\\ -\eta_3 & \eta_2 & -\eta_1 & \eta_0\end{bmatrix}$$

The error quaternion that rotates the current body frame to the desired body frame as shown in Fig. 6 is given by

$$\eta_e=\bar{\eta}_d\circ\eta \tag{38}$$

which can be represented as

$$\eta_e=Q(\bar{\eta}_d)\eta \tag{39}$$

where

$$Q(\bar{q}_d)=\begin{bmatrix}\eta_{0d} & \eta_{1d} & \eta_{2d} & \eta_{3d}\\ -\eta_{1d} & \eta_{0d} & \eta_{3d} & -\eta_{2d}\\ -\eta_{2d} & -\eta_{3d} & \eta_{0d} & \eta_{1d}\\ -\eta_{3d} & \eta_{2d} & -\eta_{1d} & \eta_{0d}\end{bmatrix}$$

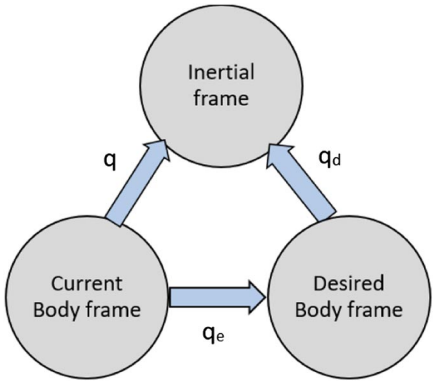

Fig. 6 Frame rotation using quaternion.

The derivative of quaternion error vector is obtained as

$$\dot{\eta}_e = \dot{\bar{\eta}}_d \circ \eta + \bar{\eta}_d \circ \dot{\eta} \tag{40}$$

The kinematic relation between quaternion and angular velocity in the desired body frame as can be written as

$$\dot{\eta}_d = \frac{1}{2}\eta_d \circ \omega_d \tag{41}$$

$$\therefore \dot{\bar{\eta}}_d = -\frac{1}{2}\omega_d \circ \bar{\eta}_d \tag{42}$$

Using quaternion relationship in Eq. (42), we can write Eq. (40) as

$$\dot{\eta}_e = \frac{1}{2}\eta_e \circ (\omega - \bar{\eta}_e \circ \omega_d \circ \eta_e) \tag{43}$$

$$\therefore \dot{\eta}_e = \frac{1}{2}\eta_e \circ (\omega - R(\eta_e)^T \omega_d) \tag{44}$$

If we define the error between the actual and desired angular velocity vector in the current body frame to be $\boldsymbol{\omega}_e$, we get

$$\boldsymbol{\omega}_e = \boldsymbol{\omega} - R(\eta_e)^T \boldsymbol{\omega}_d \quad \therefore \dot{\eta}_e = \frac{1}{2}\eta_e \circ \omega_e \tag{45}$$

Then the body angular acceleration can be related to the quaternion double derivative by differentiating Eq. (45) as

$$\ddot{\eta}_e = \frac{1}{2}(\dot{\eta}_e \circ \omega_e + \eta_e \circ \dot{\omega}_e) \tag{46}$$

where

$$\dot{\boldsymbol{\omega}}_e = \dot{\boldsymbol{\omega}} - \dot{R}(\eta_e)^T \boldsymbol{\omega}_d - R(\eta_e)^T \dot{\boldsymbol{\omega}}_d$$

The desired angular acceleration vector in the current body frame can be obtained from the above equation as

$$\dot{\boldsymbol{\omega}} = \dot{\boldsymbol{\omega}}_e + \dot{R}(\eta_e)^T \boldsymbol{\omega}_d + R(\eta_e)^T \dot{\boldsymbol{\omega}}_d \tag{47}$$

The derivative of the rotation matrix is given by

$$\dot{R}^T = -\Omega R^T$$

where $\Omega = 2G\dot{G}^T$. As the quaternion attitude dynamics is of relative degree 2 with respect to control inputs, the desired second-order closed-loop quaternion error dynamics can be chosen as

$$\ddot{\eta}_e + 2\zeta_q w_{n_q}^T \dot{\eta}_e + w_{n_q} w_{n_q}^T (\eta_e - \eta_{\text{ed}}) = 0 \tag{48}$$

where $\eta_{\text{ed}} = [1 \quad 0 \quad 0 \quad 0]^T$ is the desired error quaternion representing rotation error of 0°, and ζ_q and w_{nq} represent 4×4 diagonal matrices of the desired damping ratio and natural frequency for the quaternion attitude dynamics. Using quaternion kinematics, the relation between angular acceleration error and quaternion double derivative can be given as

$$\dot{\boldsymbol{\omega}}_e = 2G(\eta_e)\ddot{\eta}_e \tag{49}$$

where $\omega_e = \omega - \omega_d$. Then, using Eqs. (47–49), the desired angular rate dynamics can be obtained as

$$\dot{\boldsymbol{\omega}} = 2G(\eta_e)(-2\zeta_q w_{n_q}^T \dot{\eta}_e - w_{n_q} w_{n_q}^T (\eta_e - \eta_{ed})) + \dot{R}(\eta_e)^T \boldsymbol{\omega}_d + R(\eta_e)^T \dot{\boldsymbol{\omega}}_d \tag{50}$$

which can be solved using Eqs. (38) and (40). Now, solving Eq. (36) by providing desired angular acceleration from Eq. (50), we get the desired moments about the quadrotor body-fixed axes. The control allocation is discussed later in this section.

B. Transition Mode

In this subsection, the transition behavior and control strategy are discussed. The main objective of designing a transition controller is to enable the vehicle to change its flight role from vertical flight to horizontal fight and vice versa. In the flying vehicle, there are two sources of generating the forces during flight: 1) aerodynamic (by wings) and 2) propulsive (by rotors). The vertical flight is most efficiently achieved in rotary wing configurations where the thrust generated by rotors counteract the weight of the vehicle, whereas the horizontal flight is most efficiently achieved by fixed-wing configurations where most of the weight is supported by the lift generated from wings. Thus, the biplane-quadrotor model needs to go through a change in pitch orientation to achieve an efficient flight in the two different flight regimes (vertical and horizontal), starting from the vertical orientation of rotors and wings (i.e., $\theta_Q \approx 0°$) to the orientation when both are nearly horizontal (i.e., $\theta_Q \approx -90°$) to enable the wings to generate the lift. Hence, we command a gradual reduction in pitch attitude profile to achieve the transition during this phase.

As the pitch attitude of the quadrotor starts reducing from 0°, the vertical component of thrust provided by the rotors starts decreasing as well as no significant lift is initially generated by the wings until it transitions past the stall angle of attack. During the transition, the rotors/propellers go through edgewise flight, and therefore computing the lift due to prop wash is complicated. Hence, the transition phase becomes the most critical phase of the hybrid model as sufficient vertical force is required throughout this phase to support the weight. This requires a carefully designed pitch attitude profile. The initial phase of transition is controlled by the quadrotor mode controller, but the outer loop is modified such that it directly controls commanded pitch angle and altitude without x–y position control. The aerodynamic forces due to prop wash during this maneuver are computed using inflow velocity obtained from the momentum theory. During the final phase, when aerodynamic forces become significant, the control is switched to fixed-wing mode controller to complete transition.

After performing a vertical takeoff and reaching the desired altitude, the transition maneuver is initiated. The desired transition pitch attitude profile is divided into two phases: initial transition and final transition phases. In the initial transition phase, the pitch attitude is commanded to reduce linearly from hover pitch attitude, $\theta_{Q_{\text{hover}}}$, to an intermediate pitch attitude, $\theta_{Q_{\text{sw}}}$. The selection of $\theta_{Q_{\text{sw}}}$ depends on the wing stall angle of attack and the desired flight path angle in forward flight. Hence, switching from quadrotor to fixed-wing mode is done only when the wings have reached α_{stall}, that is, $\theta_{Q_{\text{sw}}} = \alpha_{\text{stall}} + \gamma_{\text{des}} - 90°$. Because the UAV operates in the stall region of the lift curve during this phase and the forward velocity is very small, the aerodynamic forces are mainly due to prop wash. The vertical component of thrust is the dominant force in the initial transition phase that supports weight. Hence, we apply quadrotor

mode controller discussed in the previous subsection with some modification to control the initial phase of transition. As the pitch attitude profile is controlled during this phase along with altitude, the outer loop control for x and y position is disabled. Also, unlike quadrotor mode, the desired thrust during this phase is calculated only depending on the desired vertical acceleration. As the initial transition phase is active only for 3 seconds during which the attitude transition to $\theta_{Q_{sw}}$ is achieved, it does not introduce any significant x and y position errors. Therefore, the process of transition becomes simplified. Similarly, for the transition from forward to vertical flight to achieve vertical landing, the pitch angle is commanded to gradually increase from $\theta_{f\text{trim}}$ to $\theta_{v\text{trim}}$ to perform vertical landing at desired vertical velocity.

C. Fixed-Wing Mode

As the forward flight phase is a conventional fixed-wing airplane mode, it is easier to visualize this mode by following the conventional right-hand fixed-wing axes system. However, the variables defining the dynamic model of biplane-quadrotor vehicle in Eqs. (1) and (2) are defined with respect to the quadrotor axes. Hence, the variables that are measured and fed back to the controller are the same quadrotor axes variables. To facilitate control design during the horizontal flight regime, we need to transform the dynamic variables from quadrotor axes to fixed-wing axes. According to Fig. 2, the transformation matrix, which transforms a vector in quadrotor frame to fixed-wing frame, can be defined as

$$\begin{bmatrix} v_x \\ v_y \\ v_z \end{bmatrix}_W = R_Q^W \begin{bmatrix} v_x \\ v_y \\ v_z \end{bmatrix}_Q \tag{51}$$

where

$$R_Q^W = \begin{bmatrix} 0 & 0 & -1 \\ 0 & 1 & 0 \\ 1 & 0 & 0 \end{bmatrix} \tag{52}$$

Note that $R_Q^W R_Q^{WT} = I$ and $R_W^Q = R_Q^{W-1}$. Hence, the body angular rates, body translational velocities, and inertia matrix in the fixed-wing frame can be calculated from the corresponding quantities defined in quadrotor axes using Eq. (51). The quaternion attitude in the fixed-wing frame can be calculated by integrating the quaternion kinematics relation of Eq. (3)

$$\begin{bmatrix} \dot{\eta}_0 \\ \dot{\eta}_1 \\ \dot{\eta}_2 \\ \dot{\eta}_3 \end{bmatrix}_W = \frac{1}{2} \begin{bmatrix} -\eta_1 & -\eta_2 & -\eta_3 \\ \eta_0 & -\eta_3 & \eta_2 \\ \eta_3 & \eta_0 & -\eta_1 \\ -\eta_2 & \eta_1 & \eta_0 \end{bmatrix}_W \begin{bmatrix} p \\ q \\ r \end{bmatrix}_W \tag{53}$$

The initial condition for this integration is provided by the final values of the quadrotor mode with the quaternion attitude vector rotated by $\pi/2$. The aerodynamic angle α is defined with respect to wing and is given by

$$\alpha = \tan^{-1}\left(\frac{w_W}{u_W}\right)$$

The control law for the forward flight mode is designed with an inner–outer loop structure and details are given next. The outer loop computes the desired thrust, pitch, and heading angles for controlling x–y position and forward velocity.

1. Outer Loop

In addition to thrust and gravity forces, aerodynamic forces have significant contribution to the total force acting on the body in fixed-wing mode because of higher speed of operation during forward flight. Hence, it needs to be included in the control design. The outer loop computes the desired thrust, pitch, and heading angles for controlling x–y position and forward velocity. From the specified desired outer loop inertial velocity, u_{d_W} can be obtained using Eq. (4):

$$u_{d_W} = (\eta_{0_W}^2 + \eta_{1_W}^2 - \eta_{2_W}^2 - \eta_{3_W}^2)\dot{x}_d + (2\eta_{1_W}\eta_{2_W} + 2\eta_{3_W}\eta_{0_W})\dot{y}_d + (2\eta_{1_W}\eta_{3_W} - 2\eta_{2_W}\eta_{0_W})\dot{z}_d \tag{54}$$

The throttle input to achieve desired velocity, u_{d_W}, can be obtained from the first-order stable error dynamics as follows:

$$\sigma_t = \frac{1}{g_u}(\dot{u}_{d_W} + K_u(u_{d_W} - u_W) + q_W w_W + g\sin(\theta_W) - (F_{ax_W}/m)) \tag{55}$$

where F_{ax_W} is the total aerodynamic force acting along the X_W axis. The desired thrust control input is given by

$$T = \sigma_t T_{\max} \tag{56}$$

The desired heading angle can be calculated using the stable first-order x–y position error dynamics as

$$\psi_{d_W} = \tan^{-1}\left(\frac{\dot{y}_d + k_y(y_d - y)}{\dot{x}_d + k_x(x_d - x)}\right) \tag{57}$$

The desired inner loop attitude angles can be calculated as [33]

$$\theta_{d_W} = \sin^{-1}\left(\frac{\dot{h}_d - k_h(h - h_d)}{\sqrt{a_h^2 + b_h^2}}\right) + \tan^{-1}\left(\frac{b_h}{a_h}\right) \tag{58}$$

where $a_h = u_W$ and $b_h = v_W \sin\phi_W + w_W \cos\phi_W$. The desired bank angle for coordinated turn can be obtained from stable β error dynamics with $\beta_d = 0$ as follows:

$$\phi_{d_W} = \sin^{-1}\left(\frac{r_W u_W - p_W w_W - (F_{ay_W}/m) + \dot{V}\sin\beta - k_b\beta V\cos\beta}{g\cos\theta_W}\right) \tag{59}$$

The desired quaternion vector in the wing frame can now be determined as

$$\eta_{d_W} = \begin{bmatrix} \cos(\phi_{d_W}/2)\cos(\theta_{d_W}/2)\cos(\psi_{d_W}/2) + \sin(\phi_{d_W}/2)\sin(\theta_{d_W}/2)\sin(\psi_{d_W}/2) \\ \sin(\phi_{d_W}/2)\sin(\theta_{d_W}/2)\cos(\psi_{d_W}/2) - \cos(\phi_{d_W}/2)\sin(\theta_{d_W}/2)\sin(\psi_{d_W}/2) \\ \cos(\phi_{d_W}/2)\sin(\theta_{d_W}/2)\cos(\psi_{d_W}/2) + \sin(\phi_{d_W}/2)\cos(\theta_{d_W}/2)\sin(\psi_{d_W}/2) \\ \cos(\phi_{d_W}/2)\cos(\theta_{d_W}/2)\sin(\psi_{d_W}/2) - \sin(\phi_{d_W}/2)\sin(\theta_{d_W}/2)\cos(\psi_{d_W}/2) \end{bmatrix} \tag{60}$$

2. Inner Loop

The inner-loop rigid body attitude dynamics remains the same in the fixed-wing mode as in the VTOL mode except that the total moment acting on the UAV is the sum of moments due to aerodynamic forces and thrust. The dynamics with respect to the fixed-wing frame is given by

$$(\tau_a + \tau_t)_W = I_W\dot{\boldsymbol{\omega}}_W + \boldsymbol{\omega}_W \times I_W\boldsymbol{\omega}_W \tag{61}$$

$$\boldsymbol{\omega}_W = 2G(\eta_W)\dot{\eta}_W \tag{62}$$

where τ_a is defined in Eq. (29). Similar to the quadrotor mode, the desired body rates in this mode can be computed as follows:

$$\dot{\boldsymbol{\omega}}_W = 2G(\eta_{e_W})(-2\zeta_q w_{n_q}^T \dot{\eta}_{e_W} - w_{n_q} w_{n_q}^T(\eta_{e_W} - \eta_{\mathrm{ed}_W})) + \dot{R}(\eta_{e_W})^T \boldsymbol{\omega}_{d_W} + R(\eta_{e_W})^T \dot{\boldsymbol{\omega}}_{d_W} \tag{63}$$

The desired moments in the fixed-wing frame can now be calculated from Eqs. (61) and (63) as

$$\tau_{t_W} = I_W \dot{\boldsymbol{\omega}}_W + \boldsymbol{\omega}_W \times I_W \boldsymbol{\omega}_W - \tau_a \tag{64}$$

After the initial transition phase, the remaining transition to the desired trim pitch angle, $\theta_{W_{\mathrm{trim}}}$, is achieved by the fixed-wing mode controller. The final phase of transition is also commanded to take place at the same altitude.

D. Control Allocation

During the quadrotor mode, as shown in Fig. 2, rolling and pitching moments are obtained by the product of differential thrust (left/right and front/back, respectively) and respective moment arms. The yawing moment is obtained from Eq. (15), in which the contribution of blade drag to total torque is independent of thrust and hence remains constant at all times and cancels out for four rotors. The expressions for total forces and moments due to thrust during quadrotor mode are given as

$$T = K(C_{T_1} + C_{T_2} + C_{T_3} + C_{T_4}) \tag{65}$$

$$\bar{L}_t = Kd(C_{T_1} - C_{T_2} - C_{T_3} + C_{T_4}) \tag{66}$$

$$M_t = Kd(C_{T_1} + C_{T_2} - C_{T_3} - C_{T_4}) \tag{67}$$

$$N_t = \frac{KR}{\sqrt{2}}\left(C_{T_1}^{3/2} - C_{T_2}^{3/2} + C_{T_3}^{3/2} - C_{T_4}^{3/2}\right) \tag{68}$$

The expressions for total forces and moments due to thrust during the fixed-wing mode are given as

$$T = K(C_{T_1} + C_{T_2} + C_{T_3} + C_{T_4}) \tag{69}$$

$$\bar{L}_t = -\frac{KR}{\sqrt{2}}\left(C_{T_1}^{3/2} - C_{T_2}^{3/2} + C_{T_3}^{3/2} - C_{T_4}^{3/2}\right) \tag{70}$$

$$M_t = Kd(C_{T_1} + C_{T_2} - C_{T_3} - C_{T_4}) \tag{71}$$

$$N_t = Kd(C_{T_1} - C_{T_2} - C_{T_3} + C_{T_4}) \tag{72}$$

The control allocation loop works in similar way for all three flight modes. For the desired T_d, $\bar{L}_{t_d}$, M_{t_d}, and N_{t_d}, the task is to find $C_{T_i}, \forall\ i, i = 1, 2, 3, 4$, by solving Eqs. (65–68) or Eqs. (69–72). It can be seen that Eqs. (68) and (70) are not rational; therefore, it is difficult to explicitly obtain the values of C_{T_i}. To overcome this problem, an additional loop that computes the desired rate of change of thrust coefficients is used [29]. The control allocation loop determines $U = [\dot{C}_{T_1} \quad \dot{C}_{T_2} \quad \dot{C}_{T_3} \quad \dot{C}_{T_4}]^T$ that drives $[T \quad \bar{L}_t \quad M_t \quad N_t]$ to $[T_d \quad \bar{L}_{t_d} \quad M_{t_d} \quad N_{t_d}]$. The control allocation loop is designed by choosing the first-order error dynamics for thrust and moments as follows:

$$\begin{bmatrix} \dot{T} \\ \dot{\bar{L}} \\ \dot{M} \\ \dot{N} \end{bmatrix} = \begin{bmatrix} k_t(T_d - T) \\ k_l(\bar{L}_{t_d} - \bar{L}_t) \\ k_m(M_{t_d} - M_t) \\ k_n(N_{t_d} - N_t) \end{bmatrix} \tag{73}$$

where $k_t, k_l, k_m, k_n > 0$ are gains. During the quadrotor mode, $\dot{C}_{T_i}$ are computed using Eqs. (65–68) and (73) as follows:

$$\begin{bmatrix} \dot{C}_{T_1} \\ \dot{C}_{T_2} \\ \dot{C}_{T_3} \\ \dot{C}_{T_4} \end{bmatrix} = \begin{bmatrix} K & K & K & K \\ Kd & -Kd & -Kd & Kd \\ Kd & Kd & -Kd & -Kd \\ \frac{3KR}{2}\sqrt{\frac{C_{T1}}{2}} & -\frac{3KR}{2}\sqrt{\frac{C_{T2}}{2}} & \frac{3KR}{2}\sqrt{\frac{C_{T3}}{2}} & -\frac{3KR}{2}\sqrt{\frac{C_{T4}}{2}} \end{bmatrix}_Q^{-1} \begin{bmatrix} \dot{T} \\ \dot{\bar{L}} \\ \dot{M} \\ \dot{N} \end{bmatrix}_Q \tag{74}$$

During the fixed-wing mode, $\dot{C}_{T_i}$ are computed using Eqs. (64) and (69–73) as follows:

$$\begin{bmatrix} \dot{C}_{T_1} \\ \dot{C}_{T_2} \\ \dot{C}_{T_3} \\ \dot{C}_{T_4} \end{bmatrix} = \begin{bmatrix} K & K & K & K \\ -\frac{3KR}{2}\sqrt{\frac{C_{T1}}{2}} & \frac{3KR}{2}\sqrt{\frac{C_{T2}}{2}} & -\frac{3KR}{2}\sqrt{\frac{C_{T3}}{2}} & \frac{3KR}{2}\sqrt{\frac{C_{T4}}{2}} \\ Kd & Kd & -Kd & -Kd \\ Kd & -Kd & -Kd & Kd \end{bmatrix}_W^{-1} \begin{bmatrix} \dot{T} \\ \dot{\bar{L}} \\ \dot{M} \\ \dot{N} \end{bmatrix}_W \tag{75}$$

Once virtual control input $U = [\dot{C}_{T_1} \quad \dot{C}_{T_2} \quad \dot{C}_{T_3} \quad \dot{C}_{T_4}]^T$ is obtained, it is integrated with the system dynamics to obtain the thrust coefficients. For the given thrust coefficients, the desired blade pitch angle can be obtained by solving Eq. (14).

E. Gain Tuning

The dynamical model of an aircraft having fewer actuators than DOF inherently involves time scale separation of rotational and translational motion. Such systems can exploit cascaded loop control to ensure stability of both slower (translational) and faster (rotational) dynamics. The stability and performance of cascaded loop control is decided by the individual bandwidths of each successive loop [34]. To ensure position and attitude tracking, the inner loop must have higher bandwidth compared with the outer loop. This implies that the settling time of the inner loop must be small compared with the outer loop in the time domain. The proposed control design uses a three-loop structure that requires gain selection such that the aforementioned condition on the settling time is satisfied. The settling time of first- and second-order systems is given by 4τ, where τ is the time constant. For a first-order system, $\tau = 1/K$, where K is the proportional gain. For a second-order system, $\tau = 1/\zeta\omega_n$ for the underdamped system, $\tau = 1/\omega_n$ for the critically damped system, and $\tau = 1/(\zeta - \sqrt{\zeta^2 - 1})\omega_n$ for the overdamped system, where ζ and ω_n are the damping ratio and natural frequency of desired second-order error dynamics, respectively. The settling time of control allocation loop is limited by the rate of actuation of blade pitch angle by servos. Hence, this decides the gains of control allocation loop. The gains of inner and outer loops are chosen such that they meet the settling time criteria.

IV. Numerical Results

In this section, the performance of the proposed controller is demonstrated through the simulation of full mission profile starting from vertical takeoff to hover, transition, forward flight, and then finally landing phase. The performance during each mode is evaluated separately and results for corresponding mode are shown. The complete 3D mission profile is also shown in the end, which

Table 3 Controller gains during vertical takeoff and hover phases

Gains	ζ_x	ω_{n_x}	ζ_y	ω_{n_y}	ζ_z	ω_{n_z}	ζ_{q_0}	$\omega_{n_{q_0}}$	ζ_{q_1}
Values	0.95	5	0.95	5	0.8	5	0.95	25	0.95
Gains	$\omega_{n_{q_1}}$	ζ_{q_2}	$\omega_{n_{q_2}}$	ζ_{q_3}	$\omega_{n_{q_3}}$	k_t	k_l	k_m	k_n
Values	25	0.95	25	0.95	25	125	125	125	125

validates the potential of the integrated controller. For simulations, the geometric and inertia parameters of biplane-quadrotor are considered as reported in Table 1. The simulations are carried out using the fourth-order Runge–Kutta method with a step size of 0.01 s. The rotors run at 3000 RPM in the quadrotor mode and 2000 RPM in the fixed-wing mode. In simulations, the desired command for the outer loop is given by users and it generates command for the inner loop. The desired trajectory is shown by dashed lines and the achieved trajectory is shown in solid lines.

A. Performance Evaluation in Hover Mode

In this subsection, the performance of the vertical takeoff and hover flight is demonstrated on the 6-DOF simulation model. The control design gains for this phase are given in Table 3. It can be seen from the table that the gains are chosen such that the settling time criteria discussed for gain tunning are met. The vehicle starts from the origin and is commanded to hover at the altitude of 200 m. The results for vertical takeoff and hover phase are presented in Figs. 7–10. At the start of simulation, the vehicle is commanded to take off from $x = 0$, $y = 0$, and $z = 0$. It is commanded to accelerate vertically from 0 to 5 m/s in the initial 5 s and then continue climbing at this constant velocity till $t = 40$ s. The desired vertical velocity is then gradually reduced to hover at the altitude of 200 m. As shown in Fig. 7, the vehicle takes off with a deviation of 0.1 m in the x position, which is due to the presence of wing lift and drag forces. However, subsequently hovering takes place at the desired altitude of 200 m after small overshoot.

Because of very low velocity during this phase, the effect of aerodynamics is only due to prop wash and that does not cause much deviations. The vehicle finally settles at the desired x–y–z position with minimal control effort. The attitude in terms of both quaternion and Euler parameters is shown in Fig. 8. The body velocity and angular rates are shown in Fig. 9. As expected, there is no major change in body attitude as the vehicle takes off vertically, and therefore the body rates are close to zero. It can be seen that the vehicle achieves the desired velocity. It is interesting to note that the vehicle flies at negative angle of attack during takeoff to balance the forces in the horizontal direction. The angle of attack profile is show in Fig. 10a. There are singularities in the alpha profile at the beginning and at around 45 s. This can be understood by observing body velocities in Fig. 9a. The values of body x and w velocities are so small and insignificant for forward flight, and therefore these singularities can be discarded. The control history is shown in Fig. 10. Unlike the conventional quadrotor, the vehicle required small pitching moment in addition to thrust force for climbing as the vehicle generates lift in horizontal direction during climb. The values of thrust coefficients are not shown for brevity, which are low and stay within their limits.

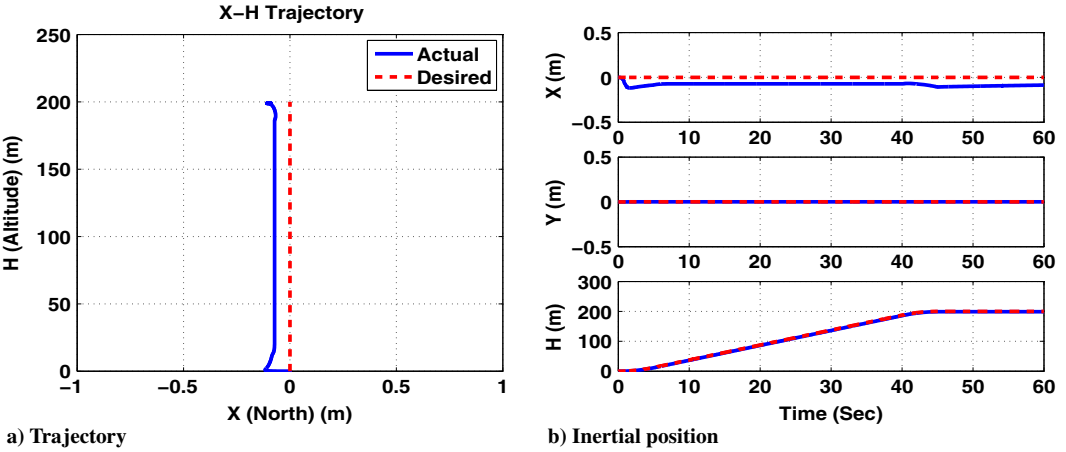

a) Trajectory b) Inertial position

Fig. 7 Vertical takeoff and hover trajectory during quadrotor mode.

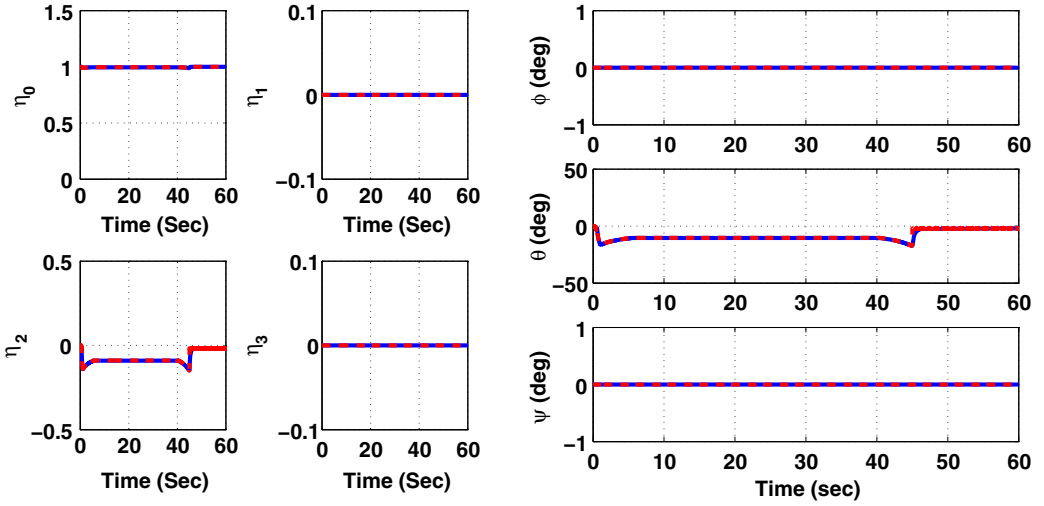

a) Quaternion attitude b) Euler angles

Fig. 8 Quaternion attitude and Euler angles during quadrotor mode.

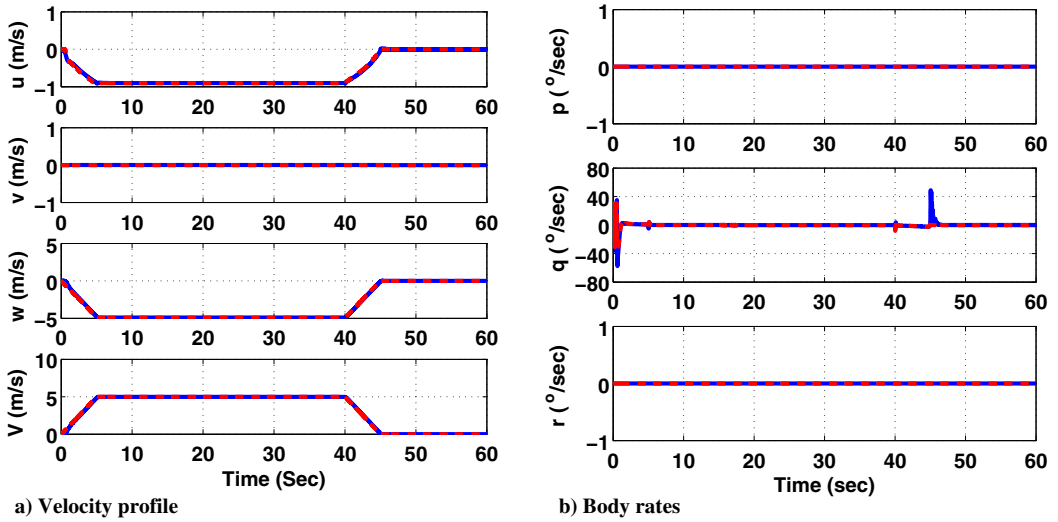

a) Velocity profile b) Body rates

Fig. 9 Velocity and body rates during quadrotor mode.

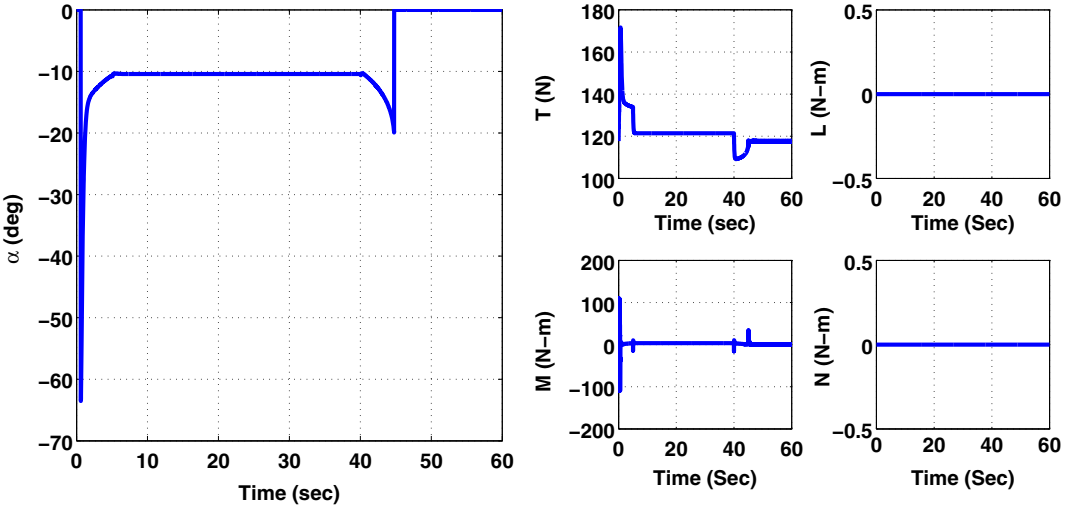

a) Angle of attack b) Control inputs

Fig. 10 Angle of attack and control inputs during quadrotor mode.

B. Performance Evaluation in Transition

In this subsection, the performance for transition from hover to forward flight phase is validated on the six DOF simulation model and the results are presented in Figs. 11–14. The control design gains for this phase are given in Table 4. It can be seen from the table that the gains meet the settling time criteria stated in the previous section. As mentioned before, the whole transition maneuver is divided into two parts: initial and final transition. The first part of transition is critical and for 3 s. In this 3 s, the pitch attitude is commanded to reduce from 0° to −78°. Second, the vehicle is asked to hold the attitude while executing this maneuver. As shown in Fig. 11, the vehicle continues to operate at the desired altitude of 200 m with little deviation during transition. However, the x position varies as the x–y position loop is disabled. The commanded pitch angle profile is depicted in Fig 12b and is well tracked.

The initial transition is critical as the vehicle has to gain enough forward speed to sustain fixed-wing flight. The vehicle gains enough velocity (from 0 m/s at hover to around 6 m/s at the end of initial transition) as shown in Fig. 13a and α reduces from post stall value to around 7° (shown in Fig. 14a), which lies in the linear region of the lift curve. The success of this maneuver depends on the ratio of maximum T/W (thrust-to-weight ratio). As the pitch attitude is reduced, the vertical component of thrust has to support weight to hold attitude and the horizontal component builds forward velocity. The control history is shown in Fig. 14. It can be seen from the figure

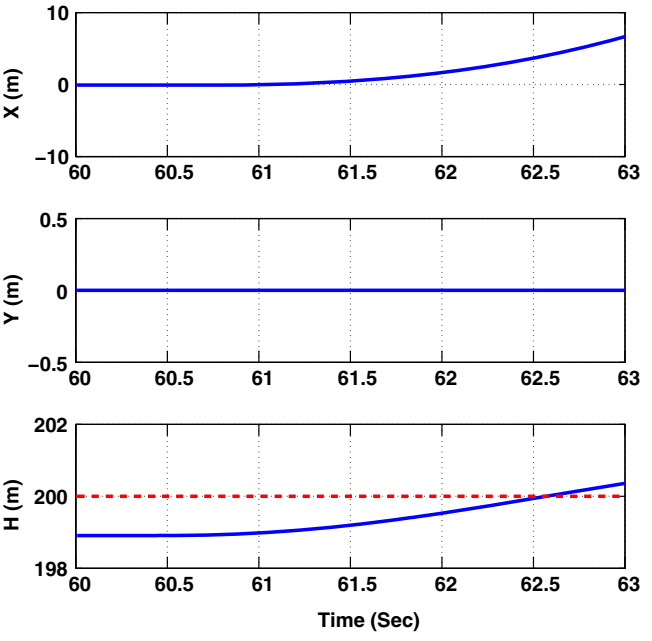

Fig. 11 Inertial position during transition phase.

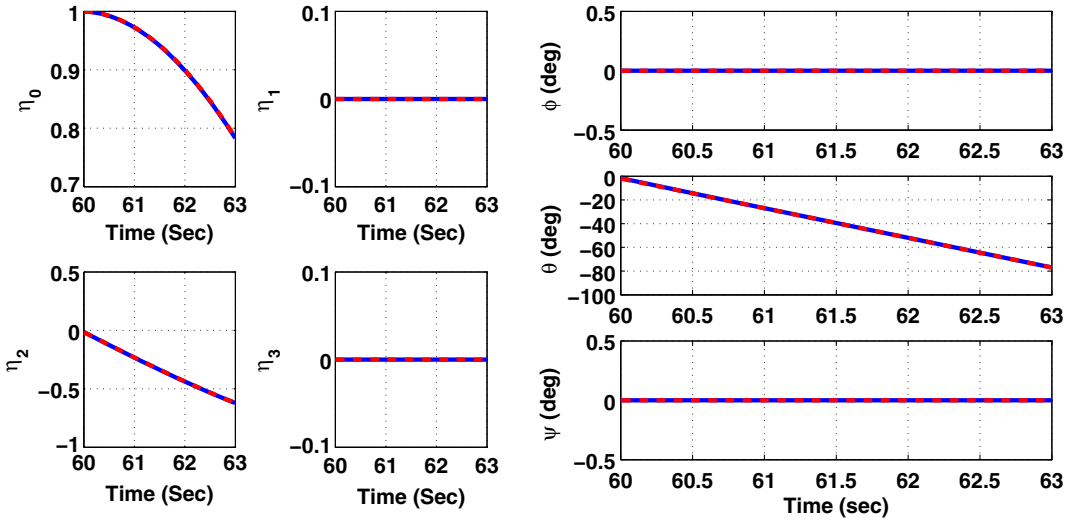

a) Quaternion attitude b) Euler angles

Fig. 12 Quaternion attitude and Euler angles during transition phase.

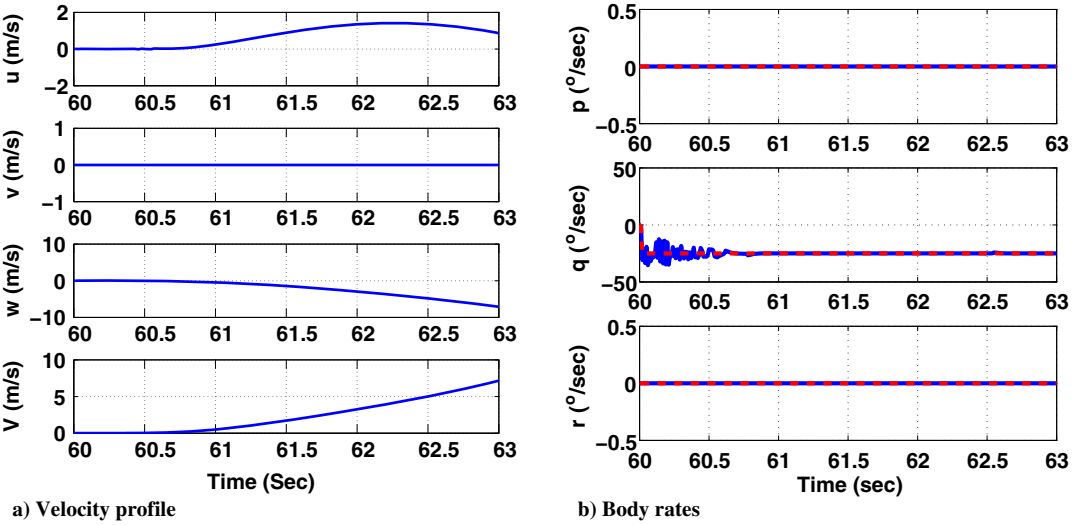

a) Velocity profile b) Body rates

Fig. 13 Velocity and body rates during transition phase.

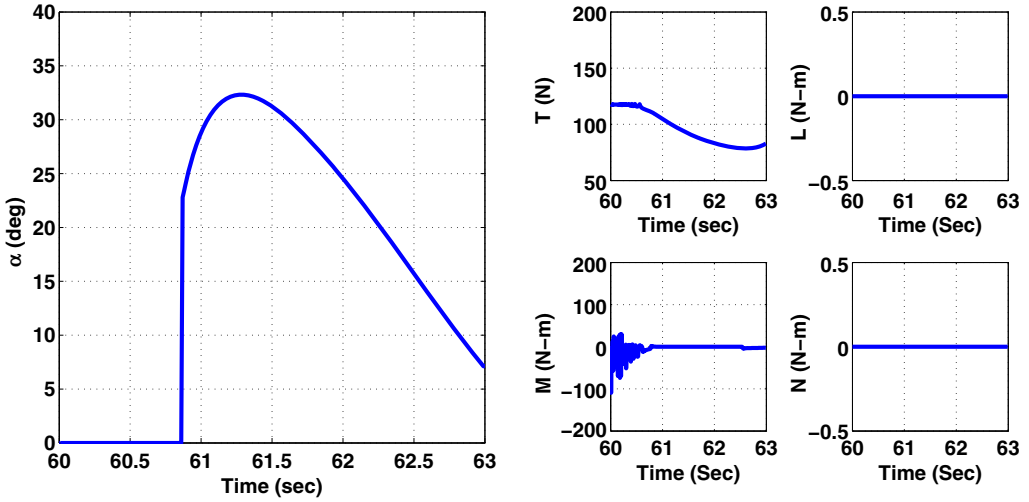

a) Angle of attack b) Desired thrust and moments

Fig. 14 Angle of attack and control history during transition phase.

that there is large requirement of thrust at the beginning, which gradually reduces as wings start generating lift. One can choose the maximum T/W to shape the transition, which we have not actively considered in our work. The profile of thrust coefficient is not provided for brevity. The coefficients stay within their limits and behave similar to control profiles. The second part of the transition is

Table 4 Controller gains during hover to forward transition

Gains	ζ_x	ω_{n_x}	ζ_y	ω_{n_y}	ζ_z	ω_{n_z}	ζ_{q_0}	$\omega_{n_{q_0}}$	ζ_{q_1}
Values	0.95	2	0.95	2	0.95	2	0.95	50	0.95
Gains	$\omega_{n_{q_1}}$	ζ_{q_2}	$\omega_{n_{q_2}}$	ζ_{q_3}	$\omega_{n_{q_3}}$	k_t	k_l	k_m	k_n
Values	50	0.95	50	0.95	50	120	120	120	120

done in the fixed-wing mode, and therefore it is clubbed with forward flight performance and demonstrated next.

C. Performance Evaluation in Forward Flight Mode

The performance of the proposed controller is validated on the 6-DOF simulation model and the results for straight and turning flight phase are presented in Figs. 15–18. The control design gains for this phase are given in Table 5. At 63 s, the fixed-wing mode controller takes over control, which completes the remaining phase of the transition and reduces pitch angle further to its trim value corresponding to desired level flight of 15 m/s. The altitude is commanded to be the same as in hover flight, that is, 200 m. The x–y position loop is enabled and is controlled by heading angle. The forward velocity is directly controlled by thrust. The altitude along with the x–y position and side slip control loops constitutes the outer loop in the fixed-wing mode and generates the pitch, yaw, and roll angle commands for the inner loop, respectively. The inner loop is designed based on quaternion error dynamics as discussed in Sec. III and generates the desired roll, pitch, and yaw moments. The control allocation loop determines thrust coefficients from the desired thrust, roll, pitch, and yaw moments. The desired values are shown with dashed lines in Figs. 15–17. It can be seen from the figures that from 63 to 90 s, the vehicle follows the desired values, which are shown with solid lines. It can be seen in Fig. 15a that y and z positions hold at the constant values up to 90 s and x increases as there is forward motion. As the desired velocity of $V_d = 15$ m/s is achieved in few second as shown in Fig 15b, the vehicle follows the x position well. The solid and dashed lines are almost on each other in Fig. 15a, and hence this demonstrates close tracking.

The vehicle settles at the desired altitude after a small initial overshoot, and the x–y trajectory tracking is performed well as shown in Fig. 15a. Also, the desired attitude and body rates tracking are achieved well as can be seen from Figs. 16 and 17. Then the vehicle is commanded to complete the final phase of transition followed by straight line following up to 90 s. A level coordinated turn of 50 s following straight line flight is commanded at 90 s and completed at 140 s. It is important to note that Figs. 15–18 show the final phase of transition, turning flight, and straight lines following together. The forward flight phase completes at 190 s. It can be seen that the altitude remains constant during the forward phase. Unlike the climb, the angle of attack is positive to support the lift. Therefore, the vehicle is efficient in forward flight. Note that the vehicle runs at reduced RPM in the forward flight. It can be seen that the thrust demand during

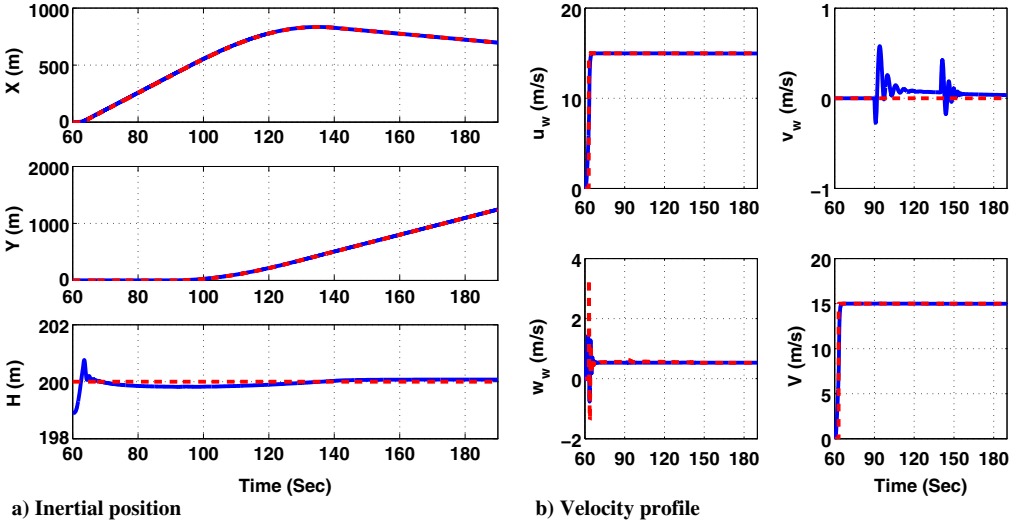

a) Inertial position b) Velocity profile

Fig. 15 Inertial position and velocity profile during forward flight phase.

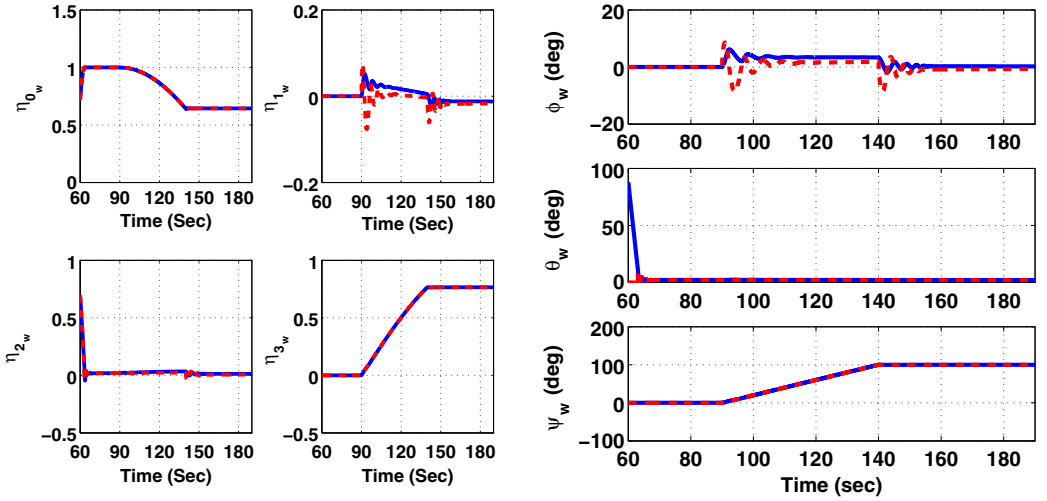

a) Quaternion attitude b) Euler angles

Fig. 16 Quaternion attitude and Euler angles during forward flight phase.

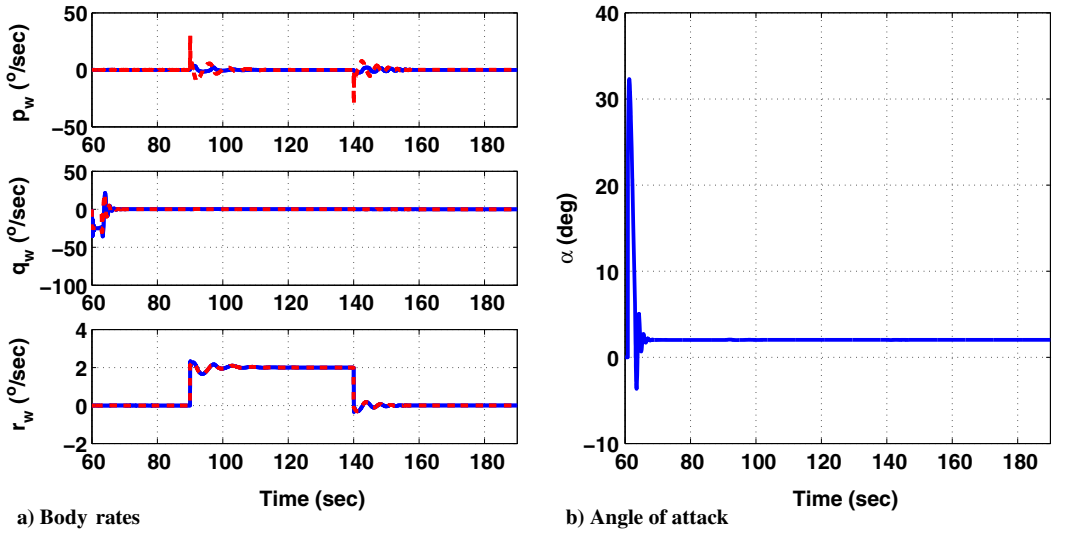

a) Body rates b) Angle of attack

Fig. 17 Body rates and angle of attack during forward flight phase.

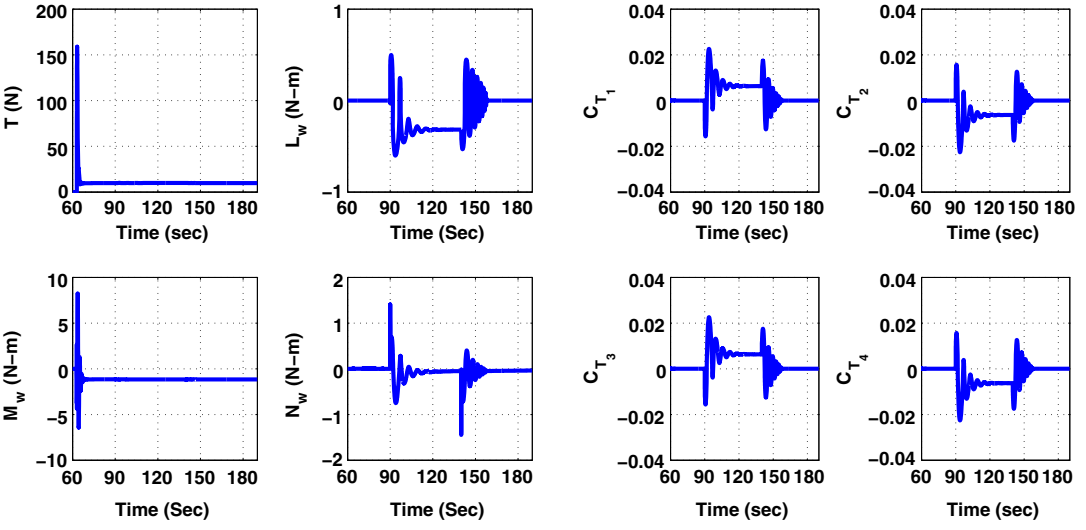

a) Desired thrust and moments b) Thrust coefficients

Fig. 18 Control history during forward flight phase.

forward flight phase is highly reduced as shown in Fig. 18, and the values of thrust coefficients are within the limits.

At 90 s, there is change in heading angle command to follow a coordinated turn. Because the vehicle does not have traditional vertical surface for stabilization, there are some oscillation in rolling and yawing moments. But the vehicle is able to maintain the desired roll angle and yaw rate (see Figs. 16b and 17a). At 140 s, there is requirement of zero roll angle to bring the vehicle to level flight. The vehicle achieves this by generating negative rolling rate and coupling between roll and yaw motion can be seen from the yaw rate requirement. As there is no dihedral and wing sweep, the vehicle experiences little oscillations before it returns to the level flight. The roll behavior could be improved by using better roll control authority. It can be observed that the comprehensive control design enables complete control over the full flight envelope and provides an effective strategy for hybrid vehicles.

Table 5 Controller gains during forward flight phase

Gains	k_x	k_y	k_h	k_β	k_u	ζ_{q_0}	$\omega_{n_{q_0}}$	ζ_{q_1}	$\omega_{n_{q_1}}$
Values	0.2	0.2	0.15	0.8	2	0.95	3	35	0.5
Gains	ζ_{q_2}	$\omega_{n_{q_2}}$	ζ_{q_3}	$\omega_{n_{q_3}}$	k_t	k_l	k_m	k_n	RPM
Values	0.95	3	35	0.5	10	35	120	35	2000

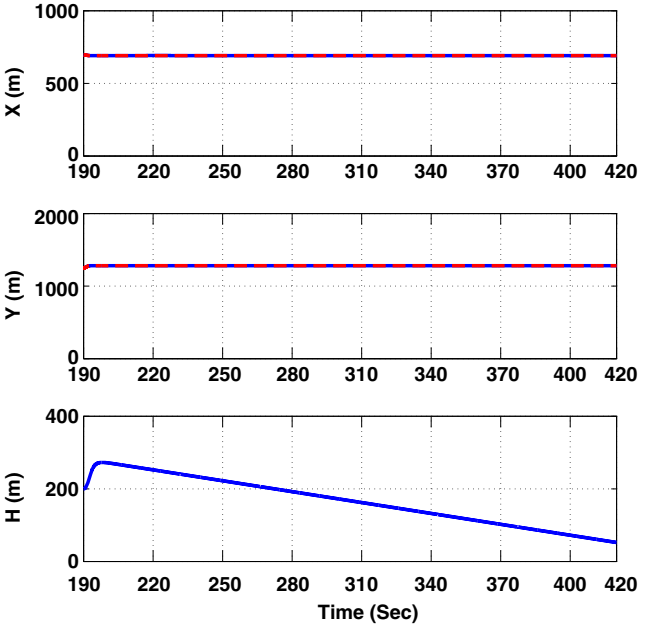

Fig. 19 Position during landing phase.

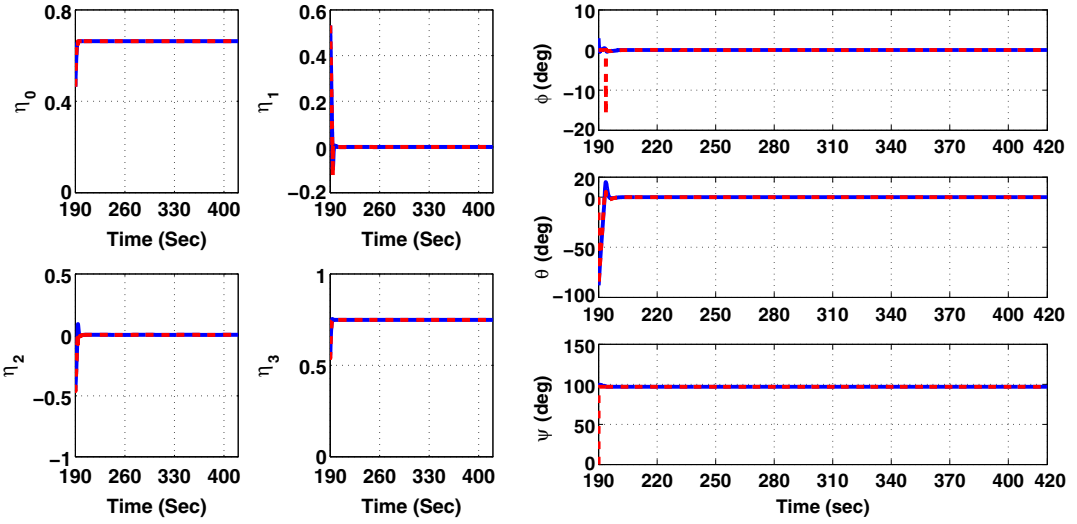

a) Quaternion attitude b) Euler angles

Fig. 20 Quaternion attitude and Euler parameters during landing.

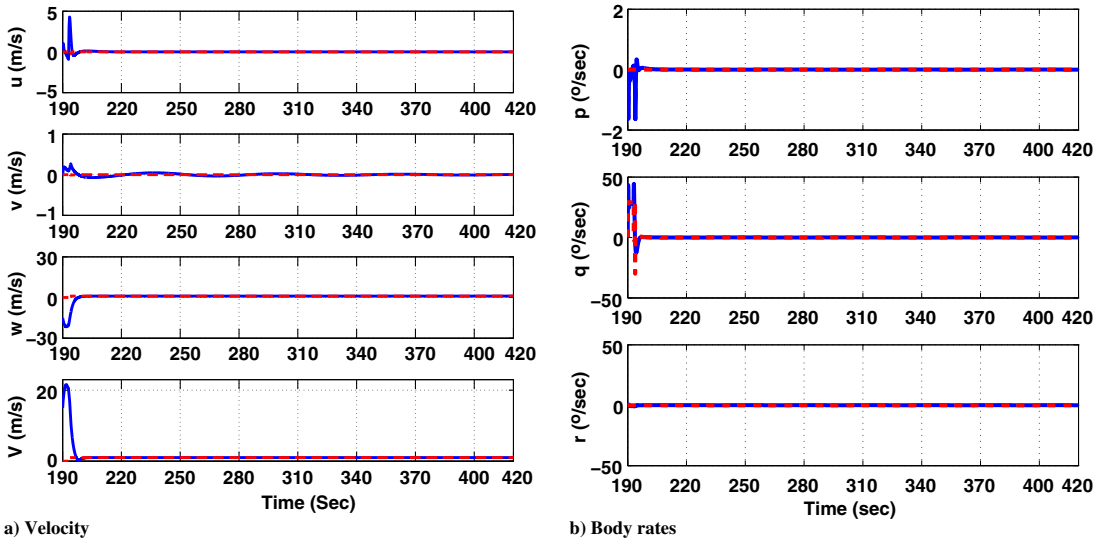

a) Velocity b) Body rates

Fig. 21 Velocity and body rates during forward to vertical landing.

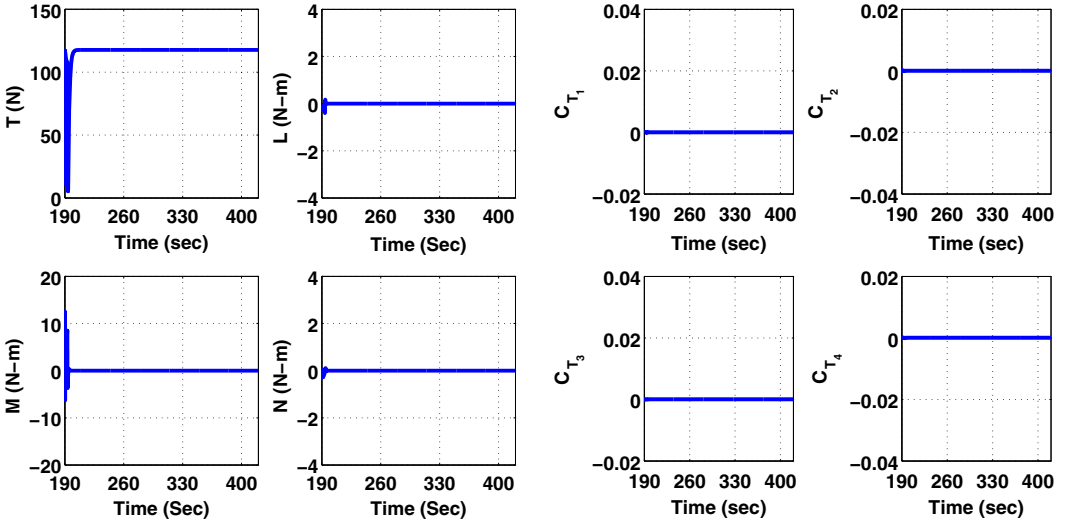

a) Desired thrust and moments b) Thrust Coefficient

Fig. 22 Control and thrust coefficient during forward to vertical landing.

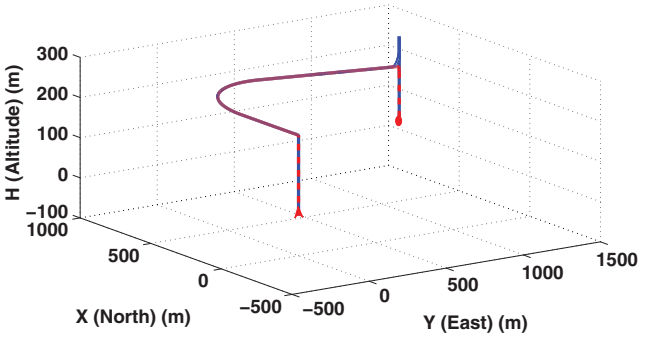

Fig. 23 Complete trajectory for the whole mission.

D. Performance Evaluation During Landing

The results for transition from forward to hover flight and landing are presented in Figs. 19–22. Unlike the forward transition, the back transition (forward to vertical flight) is completely done in the quadrotor mode as the vehicle does not require to hold forward velocity. During this phase, a gradual increase in the quadrotor pitch attitude profile is commanded for 3 s starting at 190 s. The attitude is shown in Fig. 20. It can be seen that the vehicle requires quick change in attitude that results in high body rates (can be seen in Fig. 21b) when switching to hover. The vehicle gains some altitude when it tries to pitch up for transition to hover mode. This is because kinetic energy gets transferred to potential energy. After a sudden jump in velocity due to increased RPM, velocity starts reducing. It can be seen that the thrust demand increases during transition as compared with forward flight mode as thrust has to support the weight of the vehicle as can be observed in Fig. 22. The x–y position loop is disabled during transition. Again, there is sudden jump in angle-of-attack profile due to change in mode of flight, which is not shown here as the vehicle descends at low speed.

The landing phase starts from 193 s onward such that the wing sees flow at nearly 180°. However, the vehicle speed reduces from velocity in forward flight to the desired vertically downward flight of 1 m/s. The desired landing velocity is chosen to be approximately 10% of the vehicle hover velocity. This is because the vehicle may get into vortex ring state at high descent speed [30]. As the velocity is very low, the aerodynamics effects are negligible and vehicle lands at nearly vertical flight by maintaining $T = W$ condition. The x–y position loop is again activated during landing, which helps in tracking reference x–y position to land; however, altitude is not controlled; instead, landing velocity is controlled. With the proposed strategy, the vehicle is able to quickly transition from hover to forward flight and vice versa, and therefore the strategy is effective. A complete mission profile is shown in Fig. 23.

V. Conclusions

The flight dynamics model and control strategy have been developed for a novel biplane-quadrotor tail-sitter UAV. The model describes flight dynamics, aerodynamics, rotor dynamics, and prop wash effect. The flight dynamics model has been validated with data available in the literature; therefore, the model can be used for generic representations. A set of nonlinear control laws has been developed using dynamic inversion approach for biplane-quadrotor UAV for takeoff, hover, transition, forward, and landing phases. The use of quaternions to represent the angular motion of the vehicle mitigates the singularity associated with Euler angle formulation for 90° pitch rotation of tail-sitter aircrafts. Using two different body frames of reference during vertical and horizontal flight phases enables the visualization of tail-sitter model as separate quadrotor and fixed-wing plane, and thus allows control design for the two modes in a conventional way. The complete trajectory profile of biplane-quadrotor has been controlled by combining these controllers. The efficacy of the proposed approach is shown through numerical simulations for hover, transition, and forward flight and the design is found to be satisfactory.

References

[1] Stone, R. H., Anderson, P., Hutchison, C., Tsai, A., Gibbens, P., and Wong, K., "Flight Testing of the T-Wing Tail-Sitter Unmanned Air Vehicle," *Journal of Aircraft*, Vol. 45, No. 2, 2008, pp. 673–685. doi:10.2514/1.32750

[2] Green, W. E., and Oh, P. Y., "A MAV that Flies Like an Airplane and Hovers Like a Helicopter," *Proceedings, 2005 IEEE/ASME International Conference on Advanced Intelligent Mechatronics*, Monterey, CA, 2005, pp. 693–698. doi:10.1109/AIM.2005.1511063

[3] Frank, A., McGrew, J., Valenti, M., Levine, D., and How, J., "Hover, Transition, and Level Flight Control Design for a Single-Propeller Indoor Airplane," *AIAA Guidance, Navigation, and Control Conference and Exhibit*, AIAA Paper 2007-6318, 2007. doi:10.2514/6.2007-6318

[4] Argyle, M. E., Beard, R. W., and Morris, S., "The Vertical Bat Tail-Sitter: Dynamic Model and Control Architecture," *American Control Conference (ACC), 2013*, Washington, D.C., IEEE Conference Publ., 2013, pp. 806–811. doi:10.1109/ACC.2013.6579935

[5] Sanchez, A., Escareno, J., Garcia, O., and Lozano, R., "Autonomous Hovering of a Noncyclic Tiltrotor UAV: Modeling, Control and Implementation," *IFAC Proceedings Volumes*, Vol. 41, No. 2, 2008, pp. 803–808. doi:10.3182/20080706-5-KR-1001.00138

[6] Choi, S.-W., Kang, Y., Chang, S., Koo, S., and Kim, J. M., "Development and Conversion Flight Test of a Small Tiltrotor Unmanned Aerial Vehicle," *Journal of Aircraft*, Vol. 47, No. 2, 2010, pp. 730–732. doi:10.2514/1.46180

[7] Flores, G. R., Escareño, J., Lozano, R., and Salazar, S., "Quad-Tilting Rotor Convertible MAV: Modeling and Real-Time Hover Flight Control," *Journal of Intelligent & Robotic Systems*, Vol. 65, No. 1, 2012, pp. 457–471. doi:10.1007/s10846-011-9589-x

[8] Çetinsoy, E., Dikyar, S., Hançer, C., Oner, K., Sirimoglu, E., Unel, M., and Aksit, M., "Design and Construction of a Novel Quad Tilt-Wing UAV," *Mechatronics*, Vol. 22, No. 6, 2012, pp. 723–745. doi:10.1016/j.mechatronics.2012.03.003

[9] Sobolic, F. M., "Agile Flight Control Techniques for a Fixed-Wing Aircraft," Ph.D. Thesis, Massachusetts Inst. of Technology, 2009.

[10] Khan, W., and Nahon, M., "Development and Validation of a Propeller Slipstream Model for Unmanned Aerial Vehicles," *Journal of Aircraft*, Vol. 52, No. 6, 2015, pp. 1985–1994. doi:10.2514/1.C033118

[11] Hrishikeshavan, V., Bogdanowicz, C., and Chopra, I., "Experimental Investigation of Performance of a Wing-Propeller System for a Quad-Rotor-Biplane Micro Air Vehicle," *54th Structures, Structural Dynamics, and Materials Conference*, AIAA Paper 2013-1784, April 2013. doi:10.2514/6.2013-1784

[12] Hrishikeshavan, V., Bogdanowicz, C., and Chopra, I., "Design, Performance and Testing of a Quad Rotor Biplane Micro Air Vehicle for Multi Role Missions," *International Journal of Micro Air Vehicles*, Vol. 6, No. 3, 2014, pp. 155–173. doi:10.1260/1756-8293.6.3.155

[13] Abhishek, A., Krishna, R., Sinha, S., Bhowmik, J., and Das, D., "Design, Development and Flight Testing of a Novel Quadrotor Convertiplane Unmanned Air Vehicle," *73rd American Helicopter Society Annual Forum, 2017* [CD-ROM], AHS International, Alexandria, VA, 2017.

[14] Hrishikeshavan, V., Bawek, D., Rand, O., and Chopra, I., "Development of Transition Control Methodology for a Quad Rotor-Biplane Micro Air Vehicle from Hover to Forward Flight," *The AHS International Specialists Meeting on Unmanned Rotorcraft*, AHS International, Alexandria, VA, 2013.

[15] Bogdanowicz, C., Hrishikeshavan, V., and Chopra, I., "Development of a Quad-Rotor Biplane MAV with Enhanced Roll Control Authority in Fixed Wing Mode," *71st American Helicopter Society Annual Forum 2015*, AHS International, Alexandria, VA, 2015.

[16] Chipade, V. S., Abhishek, A., Kothari, M., and Chaudhary, R. R., "Systematic Design Methodology for Development and Flight Testing of a Variable Pitch Quadrotor Biplane VTOL UAV for Payload Delivery," arXiv preprint arXiv:1801.02938, 2018.

[17] Abhishek, A., Gadekar, R., Duhoon, A., Kothari, M., Kadukar, S., Rane, L., and Suryavanshi, G., "Design, Development, and Closed-loop Flight-Testing of a Single Power Plant Variable Pitch Quadrotor Unmanned Air Vehicle," *73rd American Helicopter Society Annual Forum, 2017* [CD-ROM], AHS International, Alexandria, VA, 2017.

[18] Matsumoto, T., Kita, K., Suzuki, R., Oosedo, A., Go, K., Hoshino, Y., Konno, A., and Uchiyama, M., "A Hovering Control Strategy for a Tail-Sitter VTOL UAV That Increases Stability Against Large Disturbance," *2010 IEEE International Conference on Robotics and Automation*, Anchorage, AK, May 2010, pp. 54–59. doi:10.1109/ROBOT.2010.5509183

[19] Kita, K., Konno, A., and Uchiyama, M., "Transition Between Level Flight and Hovering of a Tail-Sitter Vertical Takeoff and Landing Aerial Robot," *Advanced Robotics*, Vol. 24, Nos. 5–6, 2010, pp. 763–781. doi:10.1163/016918610X493570

[20] Jung, Y., Shim, D. H., and Ananthkrishnan, N., "Transition Control of Near-Hover to Cruise Transition of a Tail Sitter UAV," *AIAA Atmospheric Flight Mechanics Conference*, AIAA Paper 2010-7508, Toronto, Canada, 2010. doi:10.2514/6.2010-7508

[21] Johnson, E. N., Turbe, M. A., Wu, A. D., Kannan, S. K., and Neidhoefer, J. C., "Flight Test Results of Autonomous Fixed-Wing UAV Transitions to and from Stationary Hover," *Proceedings of the AIAA Guidance, Navigation, and Control Conference Exhibit*, AIAA Paper 2006-6775, 2006. doi:10.2514/6.2006-6775

[22] Bapst, R., Ritz, R., Meier, L., and Pollefeys, M., "Design and Implementation of an Unmanned Tail-Sitter," *2015 IEEE/RSJ International Conference on Intelligent Robots and Systems (IROS)*, Hamburg, Germany, IEEE Conference Publ., 2015, pp. 1885–1890. doi:10.1109/IROS.2015.7353624

[23] Stengel, R. F., *Flight Dynamics*, Princeton Univ. Press, Princeton, NJ, 2015, Chap. 3.

[24] Stevens, B. L., Lewis, F. L., and Johnson, E. N., *Aircraft Control and Simulation: Dynamics, Controls Design, and Autonomous Systems*, Wiley, Hoboken, NJ, 2015, Chap. 2.

[25] Graf, B., "Quaternions and Dynamics," *arXiv preprint arXiv:0811.2889*, 2008.

[26] Kuipers, J., *Quaternions and Rotation Sequences: A Primer with Applications to Orbits, Aerospace and Virtual Reality*, Princeton Univ. Press, Princeton, NJ, 2002, p. 400, Chap. 11.

[27] Roskam, J., *Methods for Estimating Stability and Control Derivatives of Conventional Subsonic Airplanes*, Roskam Aviation and Engineering Corp., Lawrence, Kansas, 1971, Chaps. 3, 5, 7, 8, 9.

[28] Nelson, R., *Flight Stability and Automatic Control*, Aerospace Science & Technology, McGraw–Hill International Editions, Singapore, 1998, Chap. 3.

[29] Gupta, N., Kothari, M., and Abhishek, A., "Flight Dynamics and Nonlinear Control Design for Variable-Pitch Quadrotors," *American Control Conference (ACC), 2016*, Boston, MA, IEEE Conference Publ., 2016, pp. 3150–3155. doi:10.1109/ACC.2016.7525402

[30] Leishman, J., *Principles of Helicopter Aerodynamics*, Cambridge Aerospace Series, Cambridge Univ. Press, New York, 2002, Chap. 3.

[31] Enns, D., Bugajski, D., Hendrick, R., and Stein, G., "Dynamic Inversion: An Evolving Methodology for Flight Control Design," *International Journal of Control*, Vol. 59, No. 1, 1994, pp. 71–91. doi:10.1080/00207179408923070

[32] Prabhakaran, B., Kothari, M., and Abhishek, A., "Nonlinear Control Design for Quadrotors," *2015 IEEE Workshop on Computational Intelligence: Theories, Applications and Future Directions (WCI)*, Kanpur, India, IEEE Conference Publ., 2015, pp. 1–6. doi:10.1109/WCI.2015.7495504

[33] Ambati, P. R., and Padhi, R., "A Neuro-Adaptive Augmented Dynamic Inversion Design for Robust Auto-Landing," *IFAC Proceedings Volumes*, Vol. 47, No. 3, 2014, pp. 12202–12207. doi:10.3182/20140824-6-ZA-1003.01315

[34] Beard, R. W., and McLain, T. W., *Small Unmanned Aircraft: Theory and Practice*, Princeton Univ. Press, Princeton, NJ, 2012, Chaps. 3–5.